NMR Structures of r(GCAGGCGUGC)$_2$ and Determinants of Stability for Single Guanosine−Guanosine Base Pairs[†,‡]

Mark E. Burkard and Douglas H. Turner*

Department of Chemistry, University of Rochester, Rochester, New York 14627-0216

Received March 30, 2000; Revised Manuscript Received July 14, 2000

ABSTRACT: Nucleotides in RNA that are not Watson−Crick-paired form unique structures for recognition or catalysis, but determinants of these structures and their stabilities are poorly understood. A single noncanonical pair of two guanosines (G) is more stable than other noncanonical pairs and can potentially form pairing structures with two hydrogen bonds in four different ways. Here, the energetics and structure of single GG pairs are investigated in several sequence contexts by optical melting and NMR. The data for r(5′GCAGGCGUGC3′)$_2$, in which G4 and G7 are paired, are consistent with a model in which G4 and G7 alternate syn glycosidic conformations in a two-hydrogen-bond pair. The two distinct structures are derived from nuclear Overhauser effect spectroscopic distance restraints coupled with simulated annealing using the AMBER 95 force field. In each structure, the imino and amino protons of the anti G are hydrogen bonded to the O6 and N7 acceptors of the syn G, respectively. An additional hydrogen-bond connects the syn G amino group to the 5′ nonbridging pro-R_p phosphate oxygen. The GG pair fits well into a Watson−Crick helix. In r(5′GCAGGCGUGC3′)$_2$, the G4(anti), G7(syn) structure is preferred over G4(syn), G7(anti). For single GG pairs in other contexts, exchange processes make interpretation of spectra more difficult but the pairs are also G(syn), G(anti). Thermodynamic data for a variety of duplexes containing pairs of G, inosine, and 7-deazaguanosine flanked by GC pairs are consistent with the structural and energetic interpretations for r(5′GCAGGCGUGC3′)$_2$, suggesting similar GG conformations.

Non-Watson−Crick regions of RNA provide unique structures for recognition by proteins or therapeutic agents. For example, human immunodeficiency virus (HIV) Rev protein binds specifically to an RNA internal loop containing GA[1] and GG pairs and a bulged U (*1, 2*). Moreover, the thermodynamic stability of noncanonical regions is an important determinant of RNA folding (*3*). Studies of tandem noncanonical pairs show that thermodynamic stability and structure depend strongly on sequence (*4*−*8*). For example, tandem GA mismatches form pairs, but their stability (*4, 6*) and structure (*7, 8*) depend on the orientation of adjacent Watson−Crick pairs. Here, we explore the stability and structure of single GG pairs.

Pairs between two guanosines occur in ATP-binding aptamers found by in vitro selection (*9, 10*), in arginine and citrulline-binding aptamers (*11*), and in the core of the hepatitis δ virus (HDV) antigenomic ribozyme (*12*). As shown in Figure 1, there are four possible GG pairs that have at least two hydrogen bonds (*13*). Three of the pairings require one guanine to be flipped by backbone reversal or by a syn glycosidic torsion angle; this is indicated in Figure 1 by + signs next to both Gs. The fourth GG pair is labeled + and − (Figure 1D) and can accommodate two anti guanines in an antiparallel helix. Additional GG pairs with a bifurcated hydrogen bond linking O6 with the imino and amino protons have been observed, with small deviations from the C and D pairs in Figure 1 (*14, 15*). All GG pairings require each G to be in a distinct conformation, since even the "symmetric" pairs require one G to be flipped. Thus, interchanging G positions yields 12 possible GG configurations with two hydrogen bonds or with a bifurcated hydrogen bond, and the particular pairing may depend on context. Figure 1 also shows how the base-pair geometries compare with Watson−Crick geometry. Each C1′ for Watson−Crick geometry is shown as a black disk with a line to represent the glycosidic bond orientation. The GG structure in Figure 1C is closest to Watson−Crick geometry, with glycosidic bonds of the pair nearly aligned with those of a Watson−Crick pair.

As a single noncanonical pair in an otherwise Watson−Crick RNA helix, GG is more stable than other noncanonical pairs (*16*−*18*). In contrast with AA and UU, the single GG pair confers the same free energy in the middle of the helix

[†] This work was supported by NIH Grant GM 22939. M.E.B. is a trainee in the Medical Scientist Training Program, NIH T32 GM07356.

[‡] Coordinates of converged structures and the minimized, averaged structures have been deposited in the Research Collaboratory for Structural Bioinformatics Protein Data Bank (1F5G and 1F5H). Chemical shifts have been deposited in the BioMagResBank (4783).

* Corresponding author: phone (716) 275-3207; fax (716) 473-6889; e-mail turner@chem.rochester.edu.

[1] Abbreviations: ^{2A}P, 2-aminopurine; 7dG or 7 is 7-deazaguanosine; bp, base pair; C_T, total strand concentration in sample; dG, deoxyguanosine; dI, deoxyinosine; DQF-COSY, double-quantum filtered correlation spectroscopy; FID, free induction decay; G, guanosine; HETCOR, heteronuclear correlation spectroscopy; HPLC, high-performance liquid chromatography; I, inosine; iC, isocytosine; iG, isoguanosine; NOESY, nuclear overhauser effect spectroscopy; R, purine; *R*, gas constant, 1.987 cal·mol^{-1}·K^{-1}; rmsd, root-mean-square deviation; TBDMS, *tert*-butyldimethylsilyl; TLC, thin-layer chromatography; T_m, melting temperature in degrees Celsius, the temperature at which half of the strands are in duplex form and half are in single-stranded form; T_M, melting temperature in kelvins; t_1, the indirect time dimension in two-dimensional NMR.

10.1021/bi000720i CCC: $19.00
Published on Web 08/30/2000

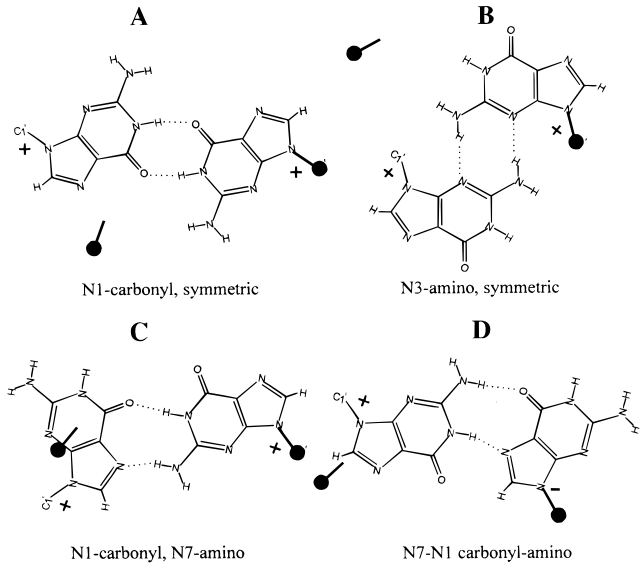

FIGURE 1: Four possible GG pairings that involve two hydrogen bonds. Structures A−C require one of the Gs to be flipped, either by a syn glycosidic torsion angle or by inverting a sugar to make a parallel backbone. The + and − signs indicate which base faces are up; for flipped base pairs, both signs are positive. For comparison, the black disks with lines overlying each pair represent C1′ atoms and glycosidic bonds in the geometry of a Watson−Crick pair. Additional GG pairs have been observed with a single bifurcated hydrogen bond linking O6 with the imino and amino protons, and are similar to the C and D pairs (*14*, *15*).

as it does near the helix terminus (*18*). When a single GG pair is placed at the center of a self-complementary RNA duplex, exchange cross-peaks in short mixing time NOESY spectra indicate that the pair is asymmetric and dynamic; by symmetry, the equilibrium constant is 1 and kinetics are slow enough at 10 °C to observe separate imino NMR resonances for guanines that exchange positions in the pairs (*18*). Mismatches of dGdG in DNA duplexes studied by one-dimensional (1D) NOE experiments also show large transfers of magnetization between imino proton resonances, consistent with exchange (*19*).

In the present work, the nature of a single GG pair in RNA is studied in several contexts. To identify functional groups important for stability, the Gs are replaced with inosine and 7-deazaguanosine, and the thermodynamics of duplex formation are obtained from ultraviolet absorbance as a function of temperature. Additional structural information is obtained by NMR. The solution structures of (5′GCAGGCGUGC3′)$_2$, which contains two single GG pairs, are modeled on the basis of restraints from NMR.

MATERIALS AND METHODS

RNA oligonucleotides were synthesized with phosphoramidite chemistry and deblocked according to published procedures (*20*−*23*). Briefly, oligomers were synthesized on an Applied Biosystems 392 DNA/RNA synthesizer. Support and phosphoramidites with 2′ TBDMS protecting groups were acquired from Glen Research (Baltimore, MD), except inosine, 7-deazaguanosine, and 2-aminopurine phosphoramidites, which were from Chemgenes, Inc. (Cambridge, MA). Oligomers were deblocked and removed from support in 3:1 (v/v) ammonium hydroxide/ethanol at 55 °C, overnight (*23*). The support was washed with water and acetonitrile, and the resulting solution was lyophilized. The 2′ TBDMS was removed with excess 1 M triethylammonium fluoride in anhydrous pyridine at 55 °C for 48 h. After desalting with a Sep-Pak C18 cartridge (Waters), the product was loaded onto a 0.5 mm silica gel TLC plate with fluorescent indicator (Baker) and developed with 55:35:10 (v/v/v) 1-propanol/ammonium hydroxide/water. Oligomers in the lowest and most intensive band were extracted with water and lyophilized. The final product was again desalted with a Sep-Pak C18 cartridge. Purity was checked by reverse-phase HPLC and was ∼95% for each oligomer.

Optical Melting Experiments. Purified oligomers were lyophilized and redissolved in 1 M NaCl, 20 mM sodium cacodylate, and 0.5 mM disodium EDTA at pH 7. Curves of absorbance at 280 nm vs temperature were acquired with a Gilford 250 spectrophotometer and a Gilford 2527 thermoprogrammer, using a heating rate of 1 °C/min. Oligomer concentration was estimated from absorbance at 280 nm and 80 °C with extinction coefficients predicted from those of dinucleoside monophosphates (*24*) by the method described by Borer (*25*). We assume 2-aminopurine contributes to the extinction similarly to adenosine; that inosine, 7-deazaguanosine, and isoguanosine contribute similarly to G; and that isocytosine contributes similarly to cytosine. Although extinctions may differ, individual bases contribute only a small portion of the oligomer extinction. Oligomers for non-self-complementary duplexes were mixed 1:1 according to the estimated concentrations. Small mixing errors do not affect thermodynamic measurements appreciably (*26*).

Melting curves were fit to a two-state model, assuming sloping linear baselines and a temperature-independent $\Delta H°$ and $\Delta S°$ (*27*). Additionally, the T_M values at different concentrations were used to calculate thermodynamic parameters according to ref *28*:

$$\frac{1}{T_M} = \frac{R}{\Delta H°}\ln (C_T/a) + \frac{\Delta S°}{\Delta H°} \qquad (1)$$

Here, a is a constant that depends on the molecularity of the reaction; $a = 1$ for self-complementary duplexes and $a = 4$ for non-self-complementary duplexes. For transitions that conform to the two-state model, $\Delta H°$ values from the two methods generally agree within 15%. The Gibbs free energy change at 37 °C was calculated as $\Delta G°_{37} = \Delta H° - (310.15)\Delta S°$.

Electronic Spectra. Absorption spectra were measured for nucleosides in 10 mM phosphate buffer at pH 7. The 7-deazaguanosine ribonucleoside was obtained from Chemgenes Corp. (Waltham, MA) and others were from Sigma.

NMR Experiments. NMR samples were lyophilized with appropriate amounts of salts. Samples for imino proton spectra were redissolved in 90:10 H_2O/D_2O. For nonexchangeable proton and ^{31}P spectra, samples were lyophilized from 99.96% D_2O and redissolved in 99.996% D_2O (Cambridge Isotope Laboratories). NMR samples contained 80 mM NaCl, 10 mM phosphate buffered to pH 7, and 0.5 mM Na_2EDTA to chelate residual divalent cations. The (5′GCAGGCGUGC3′)$_2$ sample in D_2O had a 3 mM strand concentration.

NMR spectra were acquired on a Varian Inova 500 MHz spectrometer. Imino proton spectra were acquired with a 1:3̄:3:1̄ flipback pulse sequence, to suppress water (*29*). Offset delays were selected to maximize peak intensity at 12.5 ppm.

For 1D NOE experiments, selective proton decoupling preceded the acquisition during a 3 s delay between transients. Difference spectra were obtained by subtracting from a reference spectrum, which was acquired with the decoupler set downfield of the imino resonances. Imino proton spectra were apodized with a 2 Hz line-broadening function.

NOESY spectra of samples in D_2O were acquired at various mixing times. FIDs were acquired over 256−512 complex intervals in 4K complex points with a spectral width of 4000 Hz. There were 48 or 64 scans per FID with a 3 s recycle delay. For some acquisitions, a low-power saturation was used prior to acquisition to attenuate the HDO signal.

The DQF-COSY spectrum for sugar assignments of $(5'GCA\underline{G}GC\underline{G}UGC3')_2$ was acquired at 37 °C with 512 complex intervals in 4K complex points. Spectral width was 2000 Hz, centered on the HDO resonance. For each FID, 64 scans were collected with a recycle delay of 2.5 s. The $^1H-^{31}P$ HETCOR experiment followed the method of Sklenar et al. (*30*). The spectrum was acquired at 37 °C with a spectral width of 2000 Hz in the direct, ^1H dimension, and 800 Hz in the ^{31}P dimension. FIDs were acquired in 384 complex t_1 intervals with 128 scans per interval, and 2 K complex points per FID with a recycle delay of 2 s. Two-dimensional spectra were apodized with sine bell squared functions and transformed with the Felix software package (MSI Solutions).

Proton spectra were referenced to H_2O or HDO. The temperature-dependent chemical shift of HDO was determined relative to sodium(trimethylsilyl)propionate at 0 ppm in a separate experiment. Phosphorus resonances were referenced to the phosphate peak at 0 ppm.

Restraint Generation. Distance restraints for $(5'GCA\underline{G}GC\underline{G}UGC3')_2$ were generated from 150 ms mixing time NOE volumes with pyrimidine H5/H6 cross-peaks as a reference at 2.45 Å. Other distances were calculated from the two-spin cross-relaxation approximation, with the usual r^{-6} dependence on proton−proton distance. Limits of ±30% were placed about the calculated interproton distances to allow for phasing, baseline, and noise errors in spectra, and for errors from use of a two-spin model for the more complicated multispin system.

Simulated Annealing. Structures were determined by restrained energy minimization and simulated annealing with the Discover 95 package. Starting structures were A-form and B-form RNA, with and without syn glycosidic bonds for the mismatched Gs. Calculations used the AMBER 95 force field (*31*) in addition to flat-bottom restraint potentials, with force constants of 25 kcal·mol^{-1}·Å^{-2} for distance and 50 kcal·mol^{-1}·rad^{-2} for torsion angle restraints. For electrostatics, the cell-multipole method was used with a distance-dependent dielectric constant of $\epsilon = 2r$, where r is distance in angstroms. For van der Waals interactions, group-based summation was used with an 18 Å cutoff. First, up to 500 steps of steepest-descent energy minimization was performed to relieve steric clashes or other high-energy interactions. Next, 4 ps of restrained molecular dynamics, with 1 fs time steps, was performed at 1000 K and 2 ps dynamics was run for each subsequent 100 K decrement down to 300 K. The resulting structures were minimized with up to 40 000 steps of conjugate-gradient energy minimization. Minimization calculations were stopped when either the maximum number of steps was reached or predefined convergence criteria were met. For the initial minimization and molecular dynamics, electrostatic interactions were off and van der Waals interactions were scaled to 1%. These were scaled up in 33% increments before the 700 and 600 K molecular dynamics steps and were turned on 100% for the 500 K and subsequent dynamics steps and the final energy minimization.

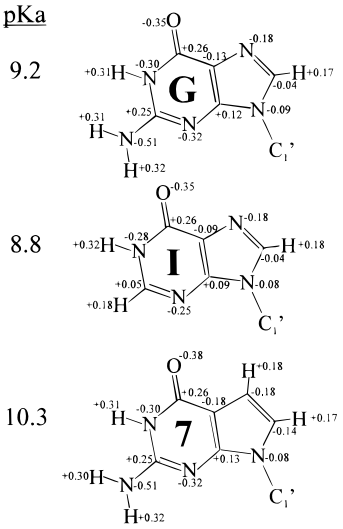

FIGURE 2: Guanine (G) and analogues inosine (I) and 7-deazaguanine (7dG). Inosine lacks the amino group, a potential hydrogen bond donor, and 7-deazaguanosine lacks N7, a potential hydrogen-bond acceptor. Löwdin partial charges were calculated with ab initio methods, using a 6-31G* basis set for 9-methyl bases and the PC-GAMESS version 4.1 software package (*32*).

Partial Charge Determination. Löwdin partial charges were determined for G, I, and 7dG by ab initio calculations of electron distributions in N9-methylated purines. Calculations were performed with the PC-GAMESS version 4.1 software package (*32*). Calculations used a 6-31G* basis set, with geometry optimization using natural internal coordinates (*33*). Solvent was assumed to be absent for calculations.

RESULTS

Functional Group Substitution. To probe possible hydrogen bonds in GG pairs, I and 7dG were substituted for guanosine (Figure 2). Inosine lacks the 2-amino group, and 7dG lacks the N7 hydrogen-bond acceptor. The effects of these analogues on the thermodynamics of duplex formation should be greatest when a functional group in a hydrogen bond is eliminated and therefore will depend on the nature of the GG pair (Figure 1). Table 1 shows thermodynamic results for pairs of G, I, and 7dG at the helix center and at two and one base pairs from the helix terminus in the context $5'G\mathbf{G}C3'$ $3'C\mathbf{G}G5'$. Table 2 presents the stabilities of these pairs calculated as

$$\Delta G^\circ_{37,\mathrm{loop}} = \Delta G^\circ_{37,\mathrm{duplex}} - \Delta G^\circ_{37,\mathrm{ref}} + \Delta G^\circ_{37,\mathrm{NN}} \quad (2)$$

where $\Delta G^\circ_{37,\mathrm{duplex}}$ and $\Delta G^\circ_{37,\mathrm{ref}}$ are the free energies for the duplexes with and without the noncanonical pair, respectively, as determined from the dependence of T_M on concentration (Table 1), and $\Delta G^\circ_{37,\mathrm{NN}}$ is the free energy

Table 1: Thermodynamics of Duplexes Containing Mismatches of Guanosine (G), Inosine (I), and 7-Deazaguanosine (*7*)[a]

	T_M dependence on concentration[b]				curve fit[c]			
duplex	$\Delta G°_{37}$ (kcal/mol)	$\Delta H°$ (kcal/mol)	$\Delta S°$ (eu)	T_m (°C) at 0.1 mM	$\Delta G°_{37}$ (kcal/mol)	$\Delta H°$ (kcal/mol)	$\Delta S°$ (eu)	T_m (°C) at 0.1 mM
3 bp from Helix End								
5′GUGGCAG3′ [d] 3′CACGGUC5′	−6.66 ± 0.01	−61.4 ± 1.2	−176.5 ± 3.9	37.7	−6.72 ± 0.04	−62.1 ± 4.2	−178.5 ± 13.5	37.9
5′GUGGCAG3′ 3′CACIGUC5′	−6.07 ± 0.03	−55.5 ± 1.8	−159.4 ± 5.9	34.5	−6.03 ± 0.07	−63.0 ± 4.8	−183.6 ± 15.3	34.6
5′GUGICAG3′ 3′CACGGUC5′	(−6.1 ± 0.02)	(−52 ± 1)	(−149 ± 4)	34.4	(−6.1 ± 0.3)	(−66 ± 13)	(−192 ± 42)	35.1
5′GUGICAG3′ 3′CACIGUC5′	−5.13 ± 0.04	−52.7 ± 1.4	−153.3 ± 4.8	29.0	−5.08 ± 0.09	−57.6 ± 5.5	−169.3 ± 17.8	29.4
5′GUGGCAG3′ 3′CAC7GUC5′	(−5.5 ± 0.03)	(−65 ± 2)	(−191 ± 5)	32.2	(−5.7 ± 0.2)	(−53.6 ± 3.0)	(−154 ± 10)	32.2
5′GUG7CAG3′ 3′CACGGUC5′	−5.68 ± 0.02	−56.6 ± 1.2	−164.0 ± 4.1	32.4	−5.71 ± 0.08	−58.1 ± 4.3	−168.7 ± 14.1	32.7
5′GUGICAG3′ 3′CAC7GUC5′	−4.71 ± 0.07	−54.9 ± 1.8	−161.7 ± 5.9	27.0	−4.69 ± 0.08	−56.5 ± 3.5	−167.1 ± 11.5	27.2
5′GUG7CAG3′ 3′CACIGUC5′	−4.91 ± 0.08	−48.9 ± 1.8	−141.7 ± 5.9	27.0	−4.67 ± 0.09	−56.3 ± 5.3	−166.4 ± 17.3	27.1
5′GUG7CAG3′ 3′CAC7GUC5′	(−2.8 ± 0.2)	(−58 ± 3)	(−176 ± 9)	17.9	(−3.6 ± 0.2)	(−43 ± 3)	(−127 ± 10)	17.5
5′GUGCAG3′ [e] 3′CACGUC5′	−7.67 ± 0.02	−55.9 ± 0.8	−155.6 ± 2.7	43.5	−7.68 ± 0.05	−56.3 ± 1.2	−156.8 ± 3.6	43.4
2 bp from Helix End								
5′CGGCAUG3′ [d] 3′GCGGUAC5′	−6.07 ± 0.02	−58.8 ± 1.9	−170.0 ± 5.9	34.6	−6.10 ± 0.09	−58.7 ± 2.6	−169.5 ± 8.2	34.7
5′CGGCAUG3′ 3′GCIGUAC5′	−5.35 ± 0.12	−60.3 ± 4.3	−177.2 ± 14.1	31.1	−5.47 ± 0.10	−56.7 ± 6.4	−165.2 ± 20.9	31.3
5′CGICAUG3′ 3′GCGGUAC5′	−5.54 ± 0.04	−55.2 ± 1.6	−160.1 ± 5.3	31.6	−5.56 ± 0.06	−56.6 ± 3.2	−164.6 ± 10.5	31.7
5′CGICAUG3′ 3′GCIGUAC5′	−4.62 ± 0.06	−55.4 ± 1.5	−163.8 ± 5.1	26.6	−4.75 ± 0.09	−52.1 ± 2.5	−152.6 ± 8.4	26.8
5′CGGCAUG3′ 3′GC7GUAC5′	−5.37 ± 0.09	−52.9 ± 3.0	−153.2 ± 9.8	30.4	−5.43 ± 0.11	−52.0 ± 3.6	−150.3 ± 11.7	30.6
5′CG7CAUG3′ 3′GCGGUAC5′	−5.42 ± 0.05	−54.0 ± 1.8	−156.8 ± 6.1	30.8	−5.50 ± 0.11	−52.4 ± 3.3	−151.3 ± 10.7	31.0
5′CGICAUG3 3′GC7GUAC5′	−4.64 ± 0.09	−48.8 ± 2.0	−142.2 ± 6.8	25.4	−4.88 ± 0.18	−43.5 ± 2.2	−124.4 ± 7.6	25.7
5′CG7CAUG3′ 3′GCIGUAC5′	(−4.2 ± 0.1)	(−55 ± 2)	(−164 ± 7)	24.2	(−4.5 ± 0.1)	(−47 ± 2)	(−138 ± 6)	24.4
5′CGCAUG3′ [e] 3′GCGUAC5′	−7.00 ± 0.03	−48.6 ± 1.7	−134.0 ± 5.4	40.1	−7.11 ± 0.14	−54.2 ± 3.1	−151.8 ± 9.6	40.3
1 bp from Helix End								
5′GGCUGAG3′ [d] 3′CGGACUC5′	−6.88 ± 0.02	−49.7 ± 1.5	−138.1 ± 4.9	39.2	−6.92 ± 0.13	−53.9 ± 3.2	−151.4 ± 10.1	39.3
5′GGCUGAG3′ 3′CIGACUC5′	−6.69 ± 0.01	−46.0 ± 0.3	−126.7 ± 1.0	38.1	−6.66 ± 0.11	−52.8 ± 1.9	−148.9 ± 6.3	37.7
5′GICUGAG3′ 3′CGGACUC5′	−6.46 ± 0.01	−46.9 ± 1.2	−130.4 ± 3.9	36.5	−6.48 ± 0.06	−50.9 ± 3.0	−143.1 ± 9.6	36.7
5′GICUGAG3′ 3′CIGACUC5′	−6.31 ± 0.03	−43.1 ± 1.4	−118.6 ± 4.5	35.4	−6.28 ± 0.09	−49.7 ± 3.7	−140.1 ± 11.7	35.5
5′GGCUGAG3′ 3′C7GACUC5′	−6.74 ± 0.01	−46.2 ± 1.1	−127.3 ± 3.4cd	38.4	−6.76 ± 0.10	−51.6 ± 3.7	−144.6 ± 11.6	38.4
5′G7CUGAG3′ 3′CGGACUC5′	−6.52 ± 0.01	−46.0 ± 1.2	−127.2 ± 3.9	36.9	−6.60 ± 0.11	−52.4 ± 3.8	−147.6 ± 12.0	37.4
5′GICUGAG3′ 3′C7GACUC5′	−6.32 ± 0.02	−45.6 ± 1.4	−126.7 ± 4.7	35.6	−6.38 ± 0.06	−48.5 ± 4.8	−135.7 ± 15.4	36.0
5′G7CUGAG3′ 3′CIGACUC5′	−6.33 ± 0.01	−48.1 ± 1.3	−134.6 ± 4.1	35.7	−6.38 ± 0.10	−50.1 ± 3.5	−141.1 ± 11.1	36.0
5′G7CUGAG3′ 3′C7GACUC5′	−6.19 ± 0.03	−44.0 ± 1.8	−121.9 ± 5.8	34.6	−6.25 ± 0.08	−45.5 ± 4.3	−126.4 ± 13.8	35.1
5′GCUGAG3′ [e] 3′CGACUC5′	−7.72 ± 0.02	−55.9 ± 0.8	−155.2 ± 2.7	43.7	−7.81 ± 0.09	−58.9 ± 2.0	−164.6 ± 6.1	43.9
Self-Complementary Duplexes								
(5′GCGICGC3′)$_2$	−7.82 ± 0.03	−65.2 ± 1.1	−185.1 ± 3.5	47.5	−7.95 ± 0.16	−68.1 ± 3.7	−194.0 ± 11.3	47.7
(5′GCGCGC3′)$_2$ [d]	−10.83 ± 0.22	−68.2 ± 3.1	−185.0 ± 9.2	62.4	10.36 ± 0.18	61.2 ± 2.9	163.8 ± 8.9	62.7
(5′CGCIGCG3′)$_2$	−6.17 ± 0.02	−51.8 ± 1.5	−147.3 ± 4.7	40.0	−6.24 ± 0.11	−54.2 ± 3.7	−154.6 ± 11.5	40.3
(5′CGCGCGp3′)$_2$ [f]	−9.12	−54.5	−146.4	57.8				
(5′GCAGGCGUGC3′)$_2$	−9.15 ± 0.03	−84.4 ± 1.2	−242.7 ± 3.9	50.3	−8.95 ± 0.08	−76.0 ± 2.4	−216.1 ± 7.8	51.0
(5′GCAGGCIUGC3′)$_2$	(−7.3 ± 0.1)	(−75 ± 3)	(−217 ± 9)	44.1	(−7.1 ± 0.1)	(−59 ± 3)	(−167 ± 9)	44.6
(5′GCAIGCGUGC3′)$_2$	(−8.5 ± 0.1)	(−53 ± 1)	(−144 ± 4)	54.1	(−9.5 ± 0.8)	(−74 ± 12)	(−208 ± 36)	53.9
(5′GCAGCUGC3′)$_2$	−13.87 ± 0.18	−88.8 ± 2.0	−241.7 ± 5.9	68.5	−13.63 ± 0.24	−86.0 ± 2.3	−233.5 ± 6.8	68.6
(5′GCGUGCAGGC3′)$_2$	−9.15 ± 0.09	−84.0 ± 2.5	−241.1 ± 7.7	50.4	−8.81 ± 0.14	−73.8 ± 3.1	−209.6 ± 9.7	50.8

Table 1 (Continued)

duplex	T_M dependence on concentration[b] $\Delta G°_{37}$ (kcal/mol)	$\Delta H°$ (kcal/mol)	$\Delta S°$ (eu)	T_m (°C) at 0.1 mM	curve fit[c] $\Delta G°_{37}$ (kcal/mol)	$\Delta H°$ (kcal/mol)	$\Delta S°$ (eu)	T_m (°C) at 0.1 mM
Self-Complementary Duplexes								
(5′GCUGCAGC3′)$_2$	−14.50 ± 0.13	−96.5 ± 1.5	−264.5 ± 4.4	68.2	−14.34 ± 0.34	−94.8 ± 3.8	−259.5 ± 11.2	68.2
(5′GC^{2A}PGGCGUGC3′)$_2$	−9.33 ± 0.09	−92.6 ± 2.4	−268.5 ± 7.5	49.7	−8.94 ± 0.13	−81.3 ± 4.9	−233.1 ± 15.4	50.0
(5′GC^{2A}PGCUGC3′)$_2$	−14.57 ± 0.09	−97.1 ± 1.0	−266.2 ± 3.1	68.3	−14.37 ± 0.31	−95.1 ± 3.2	−260.4 ± 9.2	68.2
(5′GCAGiGiCGUGC3′)$_2$	−10.44 ± 0.29	−89.0 ± 5.7	−253.1 ± 17.6	54.6	−9.79 ± 0.33	−75.6 ± 3.5	−212.3 ± 10.2	54.8
(5′GCAiGiCUGC3′)$_2$	−13.85 ± 0.16	−84.1 ± 1.7	−226.4 ± 5.0	70.4	−14.22 ± 0.22	−88.2 ± 2.5	−238.5 ± 7.4	70.3
(5′GCAGICGUGC3′)$_2$	(−5.4 ± 0.1)	(−73 ± 3)	(−219 ± 11)	35.7	(−5.9 ± 0.6)	(40 ± 14)	(−110 ± 47)	38.3
(5′GCAICUGC3′)$_2$	−8.57 ± 0.09	−69.1 ± 2.3	−195.2 ± 7.0	50.6	−8.89 ± 0.27	−76.0 ± 4.5	−216.2 ± 13.7	50.7
(5′GAGGAUGCUC3′)$_2$	−7.29 ± 0.01	−83.5 ± 0.9	−245.8 ± 2.7	43.1	−7.30 ± 0.04	−79.3 ± 6.2	−232.0 ± 20.1	43.5
(5′GAGGAUICUC3′)$_2$	(−5.1 ± 0.1)	(−99 ± 3)	(−302 ± 11)	35.2	(−5.6 ±0.5)	(−55 ± 11)	(−158 ± 37)	36.4
(5′GAGIAUGCUC3′)$_2$	−5.33 ± 0.03	−77.4 ± 2.7	−232.3 ± 8.8	35.6	−5.46 ± 0.15	−69.2 ± 6.2	−205.6 ± 20.4	36.0
(5′GAGIAUICUC3′)$_2$	(−3.8 ± 0.1)	(−79 ± 5)	(−243 ± 15)	29.8	(−4.7 ±0.6)	(−48 ± 14)	(−140 ± 48)	30.7
(5′GAGAUCUC3′)$_2$[e]	−10.10 ± 0.10	−75.0 ± 1.7	−209.2 ± 5.2	56.5	−10.34 ± 0.21	−78.8 ± 3.3	−220.7 ± 10.1	56.5
(5′CGGAGCUGCG3′)$_2$	−9.36 ± 0.07	−89.1 ± 2.0	−257.2 ± 6.3	50.4	−8.94 ± 0.21	−78.0 ± 2.7	−222.6 ± 8.0	50.6
(5′CGAGCUCG3′)$_2$	−13.16 ± 0.17	−88.0 ± 2.1	−241.4 ± 6.1	65.8	−12.82 ± 0.38	−83.7 ± 4.5	−228.4 ± 13.4	65.9
(5′GCAGCGGUGC3′)$_2$	(−9.7 ± 0.2)	(−96 ± 4)	(279 ± 14)	50.4	(−8.4 ± 0.3)	(−62 ± 3)	(174 ± 10)	51.2

[a] Duplexes in parentheses deviate significantly from the two-state model, since the enthalpies determined by curve fits and by the $1/T_M$ vs ln (C_T) correlation differ by >15%. [b] Thermodynamic parameters are determined by the slope and intercept of $1/T_M$ vs ln (C_T). [c] Thermodynamic parameters are determined by fitting each melting curve and averaging. [d] Reference 18. [e] Reference *34*. [f] Reference *61*.

Table 2: $\Delta G°_{37,loop}$ for Single Mismatches in the Context $\frac{5'GXC3'}{3'CYG5'}$[a]

XY	3 bp	2 bp	1 bp
GG	−2.41 ± 0.08	−2.49 ± 0.09	−2.58 ± 0.08
GI	−1.82 ± 0.09	−1.77 ± 0.15	−2.39 ± 0.08
IG	(−1.8)[b]	−1.96 ± 0.09	−2.16 ± 0.08
II	−0.88 ± 0.09	−1.04 ± 0.10	−2.01 ± 0.09
G7	(−1.3)[b]	−1.79 ± 0.12	−2.44 ± 0.08
7G	−1.43 ± 0.08	−1.84 ± 0.10	−2.22 ± 0.08
I7	−0.46 ± 0.11	−1.06 ± 0.12	−2.02 ± 0.08
7I	−0.66 ± 0.11	(−0.6)[b]	−2.03 ± 0.08
77	(+1.5)[b]		−1.89 ± 0.09

[a] Units are kcal/mol. X is closer to the 5′ helix terminus for positioning 2 bp or 1 bp from the helix end, and is located on the top strand as listed in Table 1. [b] Values in parentheses are for duplexes that deviate significantly from the two-state model used for deriving thermodynamic parameters.

attributable to the nearest-neighbor stacking interaction disrupted by the noncanonical pair. For the duplexes in Table 2, $\Delta G°_{37,NN}$ is −3.42 ± 0.08 kcal/mol (*34*).

Table 2 shows that, at the helix center (3 bp from the end), replacement of GG with GI or IG destabilizes the duplex by ∼0.6 kcal/mol. Replacing GG with II destabilizes by ∼1.5 kcal/mol, so amino groups of both Gs of the noncanonical pair contribute to stability. Compared with I, replacement of G with 7dG has a larger effect; a single substitution reduces stability by ∼1 kcal/mol and the 7dG−7dG mismatch is over 3 kcal/mol less stable than GG. An I−7dG mismatch is nearly 2 kcal/mol less stable than GG. The 7dG results suggest that N7 groups of the guanines are also important for stability of GG. The Gs of the GG pair appear equivalent; the thermodynamic effect of a given substitution is similar for each.

A GG pair has essentially the same loop free energy whether it is one, two, or three base pairs from a helix end (*18*; Table 2). In contrast, the analogue mismatches become more stable when only one base pair from a helix end, where all mismatches in Table 2 have similar free energies. The II mismatch goes from −0.9 kcal/mol at the duplex center to −2.0 kcal/mol at 1 bp from the helix terminus, and 7dG−7dG goes from a positive free energy to nearly −2 kcal/mol as the mismatch is moved to 1 bp from the helix end.

Table 3: $\Delta G°_{37,loop}$ per Mismatch for Self-Complementary Duplexes

duplex	motif	$\Delta G°_{37,loop}$ (kcal/mol)
(5′GCGGCGC3′)$_2$[a]	5′GGC3′ 3′CGG5′	−1.89
(5′GCGICGC3′)$_2$	5′GIC3′ 3′CIG5′	−0.41
(5′CGCGGCG3′)$_2$[a]	5′CGG3′ 3′GGC5′	−1.40
(5′CGCIGCG3′)$_2$	5′CIG3′ 3′GIC5′	+0.59
(5′GCAGGCGUGC3′)$_2$	5′AGG3′ 3′UGC5′	+0.28 ± 0.10
(5′GCAGGCIUGC3′)$_2$	5′AGG3′ 3′UIC5′	(+1.2)[b]
(5′GCAIGCGUGC3′)$_2$	5′AIG3′ 3′UGC5′	(+0.6)[b]
(5′GCGUGCAGGC3′)$_2$	5′AGG3′ 3′UGC5′	+0.60
(5′GAGGAUGCUC3′)$_2$	5′GGA3′ 3′CGU5′	−0.95 ± 0.06
(5′GAGGAUICUC3′)$_2$	5′GGA3′ 3′CIU5′	(+0.2)[b]
(5′GAGIAUGCUC3′)$_2$	5′GIA3′ 3′CGU5′	+0.04 ± 0.06
(5′GAGIAUICUC3′)$_2$	5′GIA3′ 3′CIU5′	(+0.8)[b]
(5′CGGAGCUGCG3′)$_2$	5′GGA3′ 3′CGU5′	−0.45
(5′GCAGCGGUGC3′)$_2$	5′AGC3′ 3′UGG5′	(−0.2)[b,c]

[a] Reference 18. [b] Values in parentheses are for duplexes that deviate significantly from a two-state model used for determining thermodynamic parameters. [c] The reference duplex free energy is estimated from nearest neighbor parameters (*34*).

Inosine−inosine mismatches were also studied in the duplexes (5′GCGICGC3′)$_2$ and (5′CGCIGCG3′)$_2$. Thermodynamics of duplex formation are shown in Table 1 and loop free energy increments are given in Table 3. The $\Delta G°_{37,loop}$ values are −0.4 kcal/mol for (5′GCGICGC3′)$_2$ and +0.6 kcal/mol for (5′CGCIGCG3′)$_2$, less favorable than the −1.9 kcal/mol for (5′GCGGCGC3′)$_2$ and −1.4 kcal/mol for (5′CGCGGCG3′)$_2$ (*18*). The 1.5 and 2.0 kcal/mol differences are similar to those observed with GG and II in non-self-complementary duplexes (Table 2).

Base analogue substitutions for guanosine can affect the strength of hydrogen bonds that are not disrupted directly. Because a more acidic imino proton indicates a stronger hydrogen bond, inosine (pK_a 8.8) is expected to hydrogen-bond more favorably, and 7-deazaguanosine (pK_a 10.3; deoxyribose derivative; *35*) less favorably, than guanine (pK_a 9.2).

Substitutions of base analogues for guanosine can affect base stacking in addition to hydrogen bonding (*36*). Differ-

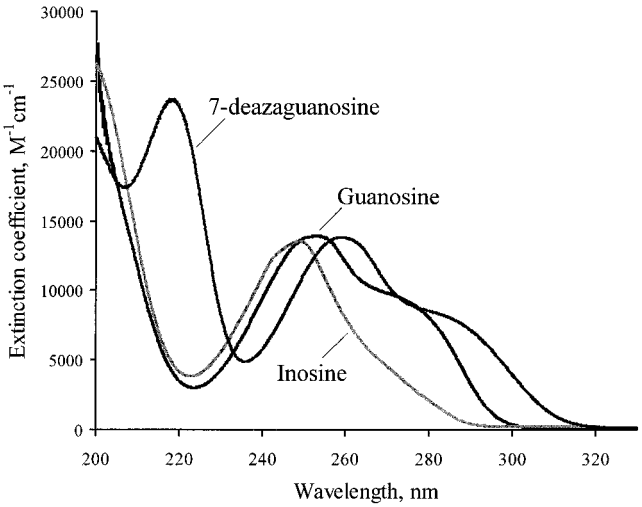

FIGURE 3: Ultraviolet absorbance spectra for guanosine, inosine, and 7-deazaguanosine ribonucleosides. Normalization was performed with reported extinction coefficients: guanosine ϵ_{253nm} = 13 910 M^{-1} cm^{-1} (*62*); inosine ϵ_{248nm} = 12 200 M^{-1} cm^{-1} (*63*); 7-deazaguanosine ϵ_{261nm} = 13 700 M^{-1} cm^{-1} (*64*).

ences in electron distribution between guanosine and its analogues can produce electrostatic and London-energy effects on stacking interactions. According to ab initio calculations, the substitutions produce only minor changes in atomic partial charges, except at the position of substitution (Figure 2). The electronic absorption spectra shown in Figure 3 provide a qualitative indication of the differences in electron distributions for these nucleosides. The guanosine spectrum indicates strong absorption near 255 nm and a broad shoulder out to 280 nm. In comparison, the inosine spectrum is shifted to the blue and lacks the shoulder at 280 nm. For 7dG, the spectrum retains the shoulder and is shifted to the red. These data indicate that there are differences in electronic distribution, which can affect stacking, but spectral shifts for I and 7dG are in opposite directions. As a first approximation, dispersion forces between molecules are related to oscillator strength divided by excitation energy (*37*), so 7-deazaguanosine is expected to produce stronger stacking, and inosine weaker stacking, than guanosine. Destabilization is observed for both I and 7dG, so the change in stacking interaction is likely to be a secondary factor in the thermodynamics of Table 2. The significant effect of these substitutions on thermodynamics suggests that hydrogen bonds are interrupted.

Imino proton NMR spectra for selected duplexes from Table 2 are shown in Figure 4. When GG is at the center of the $^{5'GUGGCAG3'}_{3'CACGGUC5'}$ duplex (Figure 4A), two sharp resonances appear around 11 ppm, corresponding to the noncanonically paired Gs. The protons in Watson−Crick pairs are above 12 ppm; at this temperature, four of these resonances are split, but they merge at higher temperatures (data not shown). The split resonances suggest slow exchange of the GG conformation, as was observed for (5′GCGGCGC3′)$_2$ (*18*). When inosine replaces one guanosine at the center of the helix, the resonance near 11.1 ppm disappears and a new resonance is observed downfield (Figure 4B). The resonances corresponding to the four split peaks in panel A are single sharp peaks in panel B. A 1D NOE experiment (Supporting Information) leads to the assignments shown. Although there is some ambiguity for other assignments, the imino proton

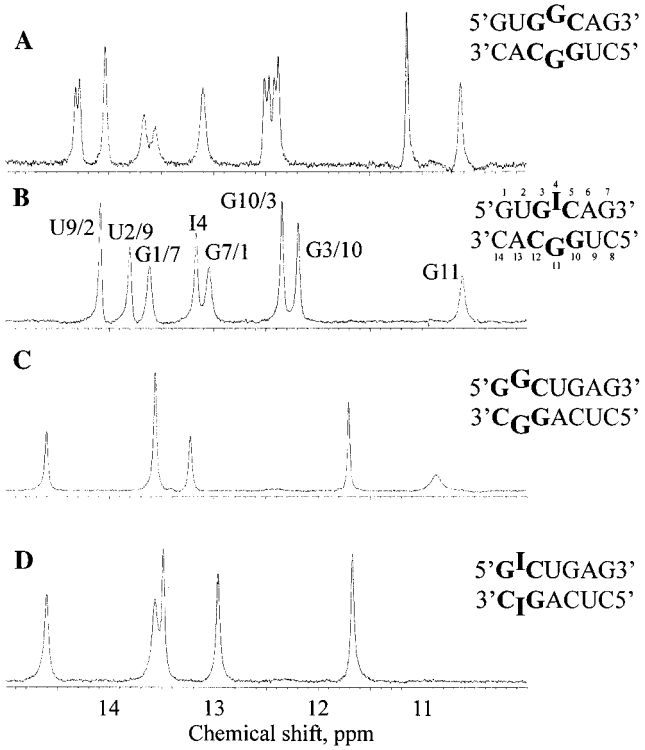

FIGURE 4: Imino proton spectra at 10 °C for the sequences indicated, which contain (A) GG 3 bp from the helix end, (B) IG 3 bp from the helix end, (C) GG 1 bp from the helix end, and (D) II 1 bp from the helix end.

at 13.2 ppm appears to belong to I4 as it has an NOE to a sharp peak at 8.3 ppm that is consistent with an inosine H2 proton. Similar downfield shifts of I imino resonances relative to G have been observed in DNA for dIdI vs dGdG pairs (*38*, *39*). The spectra for GG and II one base pair from the helix end (Figure 4C, D) each show five resonances near or above 12 ppm (in Figure 4C, the peak near 13.5 ppm represents two protons). A 1D NOE experiment for $^{5'GICUGAG3'}_{3'CIGACUC5'}$ suggests that all five peaks above 11.5 ppm correspond to Watson−Crick pairs (Supporting Information). Resonances from inosine are not observed in this context, suggesting that an II pair does not protect imino protons from exchange with water.

Self-Complementary Duplex (5′GCAGGCGUGC3′)$_2$. To accelerate or reduce conformational exchange of GG mismatches, as observed in (5′GCGGCGC3′)$_2$ (*18*) and $^{5'GUGGCAG3'}_{3'CACGGUC5'}$ (Figure 4A), and to maintain duplex symmetry preferable for NMR studies, self-complementary duplexes containing two separated GG pairs were synthesized. The (5′GCAGGCGUGC3′)$_2$ duplex provided the most useful information, apparently due to favorable fast exchange of the GG on the NMR time scale at 37 °C. Each mismatch in (5′GCAGGCGUGC3′)$_2$ has one G flanked by purines and the other flanked by pyrimidines. Table 1 contains the results of thermodynamic measurements on this duplex and derivatives with inosine at the mismatch site. Table 3 provides the $\Delta G°_{37,loop}$ values calculated according to

$$\Delta G°_{37,loop} = {}^1/_2(\Delta G°_{37,GCAGGCGUGC} - \Delta G°_{37,GCAGCUGC}) + \Delta G°_{37,NN} \quad (3)$$

where, for this duplex, $\Delta G°_{37,NN} = -2.08 \pm 0.06$ kcal/mol

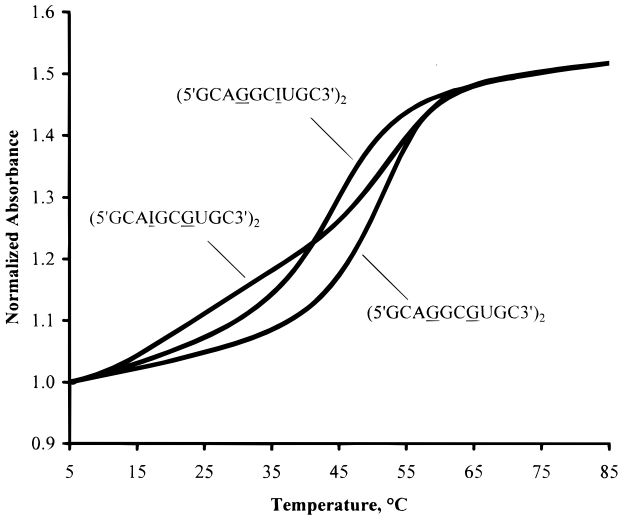

FIGURE 5: Melting curves of normalized 280 nm absorbance versus temperature for (5′GCAGGCGUGC3′)$_2$ and inosine derivatives. Calculated concentrations are 0.113 mM for 5′GCAGGCGUGC3′, 0.122 mM for 5′GCAGGCIUGC3′, and 0.092 mM for 5′GCAIGCGUGC3′. Absorbances were normalized to be the same as for 5′GCAGGCGUGC3′ at 80 °C.

for $^{5'AG3'}_{3'UC5'}$ (*34*). In this context, the loop free energy for GG is +0.3 kcal/mol at 37 °C. In contrast with the previous systems, the thermodynamic results differ significantly between IG and GI. The difference is highlighted in Figure 5, which shows melting curves for these duplexes at similar concentrations. The curve for (5′GCAGGCIUGC3′)$_2$ shows a cooperative melt with a T_m that is 6 °C lower than the duplex with the GG pair. In contrast, (5′GCAIGCGUGC3′)$_2$ shows a very broad transition from 15 to 35 °C and a sharper transition with small hypochromicity but the same T_m as with the GG pair; the approximate thermodynamic parameters of this higher temperature transition appear in Tables 1 and 3. Thus, unlike previous systems, the noncanonically paired guanosines are not equivalent in (5′GCAGGCGUGC3′)$_2$.

Figure 6 shows the imino proton spectrum and 1D NOE difference spectra for (5′GCAGGCGUGC3′)$_2$ at 30 °C. The U8 imino resonance at 13.2 ppm has an NOE to the A3H2 proton, consistent with a U imino proton in an AU pair. The two sharp resonances labeled G5 and G9 have NOEs to amino protons, consistent with imino protons in GC pairs. Additionally, the G5 imino has an NOE with G7H8 (assigned from nonexchangeable proton spectra), allowing it to be distinguished from the G9 imino proton.

Nonexchangeable Proton Assignments. The base−H1′ region of the 400 ms NOESY spectrum of nonexchangeable protons for (5′GCAGGCGUGC3′)$_2$ is shown in Figure 7. Arrows indicate sequential assignments of base and H1′ protons. The large G7H1′−H8 cross-peak (labeled G7) suggests a syn conformation about the glycosidic bond. Moreover, unusual G5H1′−G4H8 and U8H1′−G7H8 cross-peaks (labeled with asterisks) are observed, consistent with the close approach expected from a syn glycosidic torsion.

Sugar protons were assigned on the basis of the 400 ms mixing time NOESY spectrum and the DQF-COSY spectrum (Supporting Information). The ^{31}P−^{1}H HETCOR spectrum (Supporting Information) shows strong ^{31}P − H3′ coupling at most positions. Coupling cross-peaks are increasingly weak for C6H3′−G7P, G4H3′−G5P, and A3H3′−G4P; G7H3′−U8P is not observed. The proximity of the attenuated ^{31}P−^{1}H HETCOR peaks to the GG site suggests exchange broadening. Observable phosphorus resonances are contained within a 1 ppm band, suggesting that the backbone is not highly distorted near the GG pairs.

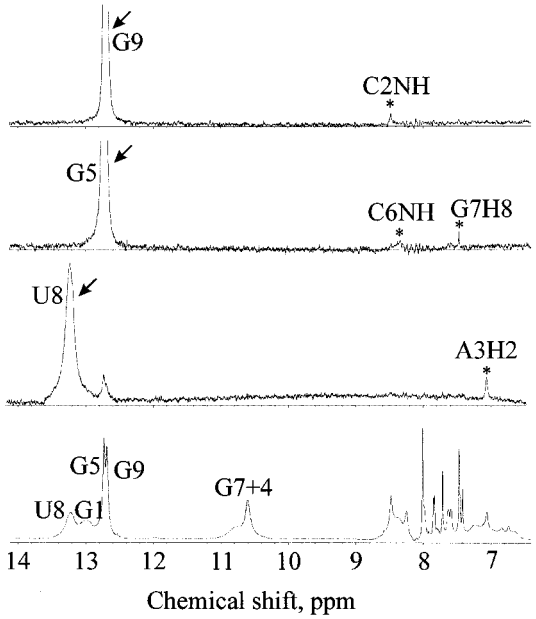

FIGURE 6: Exchangeable proton spectrum and 1D NOE difference spectra for (5′GCAGGCGUGC3′)$_2$ at 30 °C. The G7H8 resonance was assigned from spectra of nonexchangeable protons in D_2O.

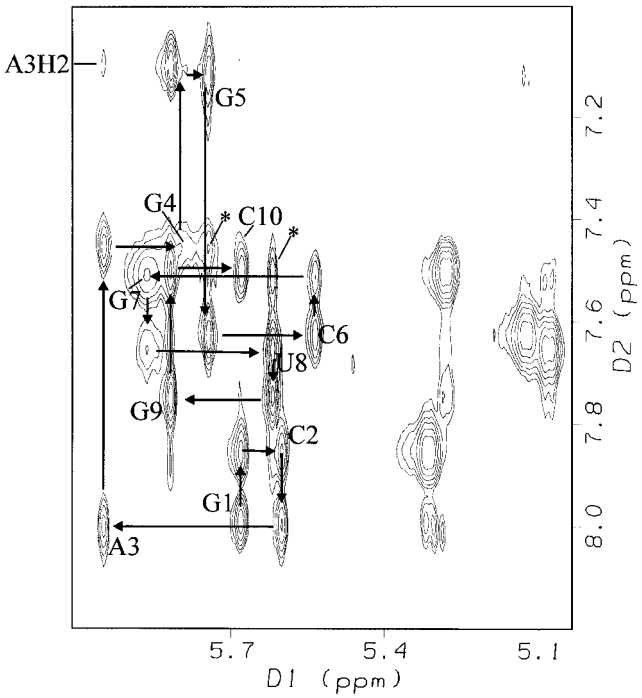

FIGURE 7: Base−H1′ region of the 400 ms NOESY spectrum for (5′GCAGGCGUGC3′)$_2$ at 37 °C. Sequential assignments of base and H1′ protons are shown by arrows. Intranucleotide H1′−H8 cross-peaks are labeled. The large volume of the G7H1′−H8 cross-peak and the presence of the U8H1′−G7H8 and G5H1′−G4H8 cross-peaks (labeled with asterisks) are consistent with syn glycosidic conformations for G4 and G7.

Assignments were not made for H5′ and H5″ of A3, G4, and G7. An NOE cross-peak from A3H2 to an unassigned aromatic proton near 7.6 ppm is also observed (Supporting Information). Although the unassigned resonance is near that

Table 4: Distance Restraints That Differed for the G4 syn and G7 syn Structures of (5′GCAGGCGUGC3′)$_2$[a]

G4 syn; G7 anti					G7 syn; G4 anti				
		distance (Å)					distance (Å)		
atom 1	atom 2	min	max	model[b]	atom 1	atom 2	min	max	model[b]
A3H2	G4H8	2.50	4.65	3.34/5.72	A3H1′	G4H8	2.72	5.05	6.64/4.91
G4H2′	G4H8	1.89	3.52	3.05/3.87	A3H2′	G4H8	2.14	3.98	5.64/2.29
G5H1′	G4H8	2.70	5.01	3.86/8.16	A3H3′	G4H8	2.18	4.05	7.92/2.75
C6H1′	G7H8	3.34	5.50	4.93/6.73	G4H3′	G4H8	1.95	3.62	4.81/2.78
C6H2′	G7H8	2.05	3.81	2.27/5.63	G5H1[c]	G7BH8	1.00	5.00	5.93/4.86
G7H3′	G7H8	1.00	5.50	2.68/4.95	G7H1′	G7H8	2.04	3.78	3.86/2.65
					G7H2′	G7H8	1.67	3.10	3.96/3.05
					U8H1′	G7H8	3.37	5.50	7.60/3.50

[a] Other restraints for both structures were identical and are provided in Supporting Information. The same set of restraints was imposed for each strand of the duplex for a given structure; only one set is shown here. [b] Distances in the minimized, averaged structure are averaged for both strands of the duplex. Distances are shown for the G4 syn structure followed by the G7 syn structure. [c] For this cross-strand restraint, G7B represents the G7 residue in the second strand. This restraint is based on strong NOE in 1D imino proton difference spectrum.

of C5H6, with closely related molecules this peak is shifted significantly from the C5H6 resonance. This unassigned resonance may reflect A3H2 in a rarely populated conformation, thus giving rise to an exchange peak with itself. Addition of 3 mM $MgCl_2$ had a minimal effect on the NOESY spectra, suggesting that the structure of the GG is unaffected by Mg^{2+}.

Restraint Generation. Distance restraints for (5′GCAGGCGUGC3′)$_2$ were obtained from NOESY peak volumes in a 150 ms mixing time spectrum. For large cross-peaks, the NOESY buildups from 50 to 150 ms were generally linear with a zero intercept, except the signal-to-noise and baseline errors were large in the 50 ms spectrum, making measurements of weak cross-peaks less reliable. Most restraints were obtained from the half of the 150 ms spectrum where the resonance with the lower chemical shift was in the direct dimension. To avoid overlap, the cross-peaks of C2H1′ and U8H1′ with other sugar protons were from the other half of the spectrum. Cross-peaks with H5′ and H5″ protons were not used for restraints.

Initial modeling suggested that restraints including the H8 protons of G4 and G7 were inconsistent with a single structure. When all restraints were included in molecular modeling, the derived structures were heterogeneous (the best five of 20 structures by energy had an average pairwise rmsd of 2.00 Å). The structures generally consisted of a stacked, anti-oriented G4 and an unstacked anti G7 in the minor groove (not shown). This structure has G4 and G7 unpaired, which is inconsistent with thermodynamic evidence. Purely anti-oriented glycosidic bonds for G4 and G7 are also inconsistent with NOESY spectra. In the best structure with all restraints included, there are 21 distance violations per strand. In light of the known dynamic nature of GG in several contexts (*18*) and the line broadening observed near the GG in (5′GCAGGCGUGC3′)$_2$, the data are most consistent with two alternating structures rather than a single structure.

It is likely that the predominant conformations of (5′GCAGGCGUGC3′)$_2$ each have either G4 or G7 in the syn glycosidic conformation; the other G is anti. The NOESY spectra are consistent with partial syn glycosidic conformations at both positions: (a) The H1′−H8 NOESY cross-peak is larger than normal for G7. (b) The unusual G5H1′−G4H8 and U8H1′−G7H8 cross-peaks (labeled with asterisks in Figure 7) are consistent with syn glycosidic conformations. (c) The A3H1′−G4H8 and C6H1′−G7H8 cross-peaks are consistent with anti glycosidic conformations, as these distances are large when glycosidic torsions are syn. (d) The G4H1′ and G7H1′ line widths are considerably broadened relative to other H1′ line widths, consistent with syn−anti exchange where the position of the purine base moves relative to the sugar.

We segregated restraints involving G4H8 and G7H8 into two sets. The first set is designated for the "G4 syn structure" and is consistent with a syn glycosidic torsion for G4 and an anti glycosidic torsion for G7, whereas the second is for the "G7 syn structure" and is consistent with an anti G4 torsion. Nonexchangeable protons other than G4H8 and G7H8 do not necessarily alter position significantly when G4 and G7 swap in the pair. Although volumes involving G4H8 and G7H8 protons are expected to be reduced due to only partial occupation of each conformation, this difference is small for purposes of developing appropriate distance restraints because distance is related to the sixth root of volume and restraints have ±30% bounds.

Table 4 contains a list of distance restraints that differ for the G4 syn and G7 syn structures; other restraints are identical (Supporting Information). Distances other than those involving G4H8 and G7H8 in the minimized, averaged structures were nearly identical for the two structures.

For the G7 syn structure, a 1.0−5.0 Å cross-strand restraint for G5H1−G7H8 is based on the NOE of Figure 6. A restraint for C6H2′ and G7H1′ to be at least 3.5 Å apart was added for both structures, since there was no observable NOE between these protons and preliminary modeling showed close approach. Hydrogen-bond restraints of 1.8−2.5 Å were used for each GC Watson−Crick pair. For the AU pair, the two hydrogen-bond restraints were set at 1.8−3.0 Å because the U imino peak is broad and at a lower chemical shift than a typical U imino in a Watson−Crick pair, although the U8H3−A3H2 NOE verifies the presence of the pair (Figure 6).

For each strand there are a total of 88 NOE distance restraints for the G4 syn structure and 90 for the G7 syn structure. These include 56/57 intranucleotide (G4 syn/G7 syn) and 32/33 internucleotide restraints. There are also 11 hydrogen-bond restraints per strand for each structure, for a total of 10.0/10.2 distance restraints per nucleotide.

Generous torsion restraints were used to maintain an approximate A-form backbone and sugar pucker (Supporting Information). The DQF−COSY spectrum provides evidence

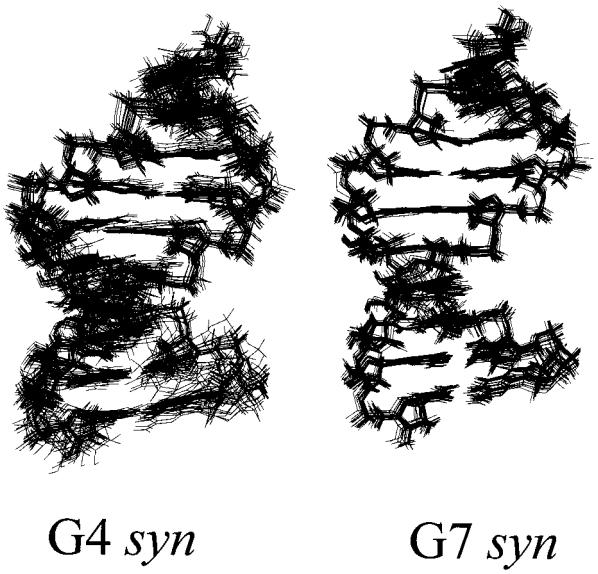

FIGURE 8: Overlap of the minimized structures with the lowest energies from the simulated annealing protocol. Left: 22 of the 25 best G4 syn structures; average pairwise rmsd is 1.07 Å. Right: the 25 best G7 syn structures; average pairwise rmsd is 0.63 Å.

for this geometry: for all nucleotides except G4 and G7, the H1′−H2′ couplings were very weak or unobservable, and H3′−H4′ was strong compared to H2′−H3′ and H4′−H5′ coupling. For G4 and G7, the H3′−H4′ couplings were weak or not observed, so restraints on sugar puckers were not used. The A3H3′−G4P and G7H3′−U8P couplings are very weak or not observed, so the ζ torsion angle was not restrained for these. Glycosidic torsion angles were loosely restrained in the anti conformation, except for G4 and G7. For the G4 syn structure, χ was restrained from −10° to +50° for G4 and −150° to +150° for G7, and these restraints were reversed for modeling the G7 syn conformation. Preliminary modeling showed that removing the syn χ restraints impairs convergence from molecular dynamics, but the optimal structures are similar with or without these restraints.

Structural Determination. For each structure, restrained molecular dynamics was performed 10 times for each of four different initial structures. The final 40 structures were sorted by energy, and the 25 with lowest energies were selected. For G4 syn, the best structures were obtained from three different initial structures: 10 from A-form with G4 anti, nine from B-form with G4 syn, and six from A-form with G4 syn. For G7 syn, there were nine from A-form with G7 anti, eight from A-form with G7 syn, six from B-form with G7 syn, and two from B-form with G7 anti.

The 25 lowest-energy structures form a population with an average pairwise rmsd of 1.07 Å for G4 syn and 0.63 Å for G7 syn. Figure 8 shows an overlay of 22 of these conformations for G4 syn and all 25 for G7 syn. Three structures for G4 syn had a disrupted GG pair and were eliminated. Overall, final energies are more favorable for the G7 syn structure than for G4 syn so, from the force field, the pair prefers the G7 syn orientation. Both duplexes of Figure 8 are in A-form helixes, but the population of molecules for G7 syn is clearly more homogeneous. An averaged conformation from these 22 or 25 conformations of Figure 8 was used as a starting point for conjugate-gradient energy minimizations, both of which converged after ~1000 steps. This yielded the final minimized, averaged structures (Figure 9).

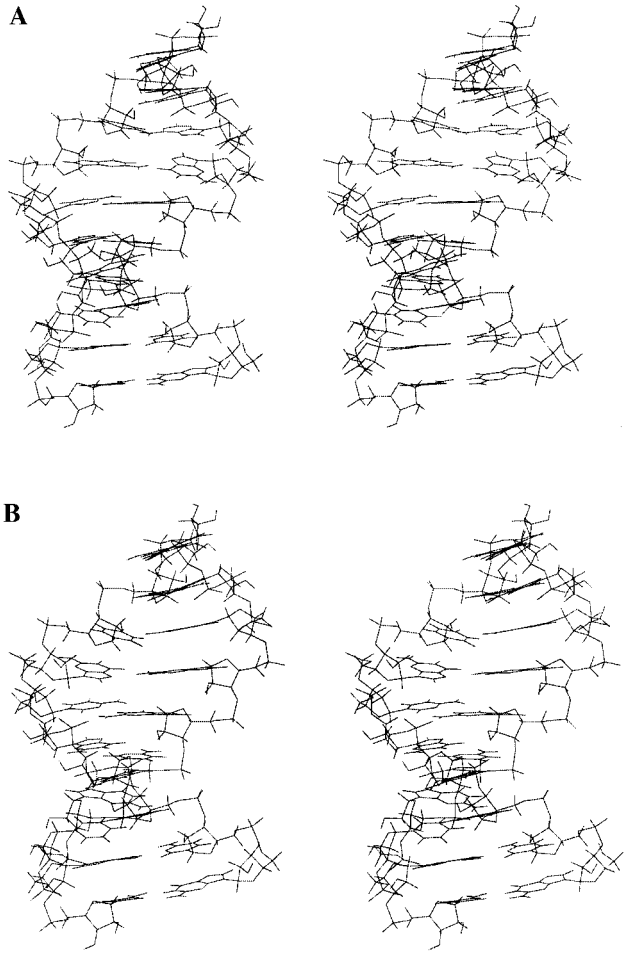

FIGURE 9: Defocused stereoviews of the minimized, averaged structures of $(5'GCA\underline{G}GC\underline{G}UGC3')_2$. (A) G4 syn structure. (B) G7 syn structure.

The final structures each contain the syn−anti N1-carbonyl, N7-amino GG pair of Figure 1C. Additionally, there is a hydrogen bond between the amino from the *syn* guanosine and the pro-R_p nonbridging oxygen of the phosphate that is 5′ of the syn G. Thus three hydrogen bonds stabilize this GG mismatch. The syn G is rotated out of the plane of the anti G for both structures (Figure 9) to accommodate the amino−phosphate hydrogen bond.

None of the Table 4 restraints are violated in the averaged, minimized structures. Overall, there are six and seven violations of intranucleotide and internucleotide restraints, respectively. An additional restraint for G5H3′−C6H6 was barely violated for G7 syn but not for the G4 syn structure. Violations are on the order of a few hundredths of an angstrom in most cases, and the maximum violation is distant from the GG site: 0.14 Å for G9H1′−C10H6 (see Supporting Information). The presence of violations indicates that, when converged, the restraint forces are necessary to oppose the force field and without the restraints, a different minimum-energy structure would be reached. A dozen small violations are, perhaps, better than a few large violations where a single tight restraint can unduly distort the structure.

The imino proton spectrum shown in Figure 6 is qualitatively consistent with these GG structures. One imino proton is in a hydrogen bond to O6 of the opposing G, protecting

Table 5: NOE Volumes for Distances That Are Expected To Be Identical for the Two Conformations of (5′GCAGGCGUGC3′)$_2$[a]

nearby in G4 syn	nearby in G7 syn	volume ratio[b]	fraction G7 syn[c]
G5H1′−G4H8	U8H1′−G7H8	3.0	0.75
G4H1′−G4H8[d]	G7H1′−G7H8	3.0	0.75
C6H1′−G7H8	A3H1′−G4H8	4.2	0.81
C6H2′−G7H8	A3H2′−G4H8	0.67	0.40

[a] Assuming that the GG pairs are equivalent for the two structures, these distances are equal, so difference in NOE volume provides a measure of conformational occupation. [b] The volume of the "nearby in G7 syn" cross-peak divided by the volume of the corresponding "nearby in G4 syn" cross-peak in the NOESY spectrum with 150 ms mixing time. [c] Estimated fraction in the G7 syn conformation from relative NOESY cross-peak volumes. [d] This cross-peak is overlapped slightly with a strong peak.

it from exchange with solvent and producing a fairly sharp resonance at 10.6 ppm. The imino proton on the other G is exposed to solvent and yields a broad resonance. In the G7 syn structure, the G7H8 proton approaches the adjacent G5 imino close enough to observe an NOE (Figure 6).

Population of G4 syn and G7 syn Conformations. Although it is difficult to obtain the relative occupation of two conformations from NOESY spectra alone (*40*), the (5′GCAGGCGUGC3′)$_2$ system has the advantage that the same GG pair is formed in each conformation. Thus, certain distances can be assumed to be equal for the two conformations. Table 5 lists four proton pairs of the G4 syn structure and the analogous pairs for G7 syn. The relative occupation of a conformation can be estimated by the relative NOE volumes of the analogous cross-peaks, and these estimates are shown in the right-hand column of Table 5. Three of four estimates are based on distances to H1′ protons and indicate that (5′GCAGGCGUGC3′)$_2$ exists in the G7 syn conformation ~75−80% of the time. The fourth estimate, based on the C6H2′−G7H8 and A3H2′−G4H8 NOE cross-peaks, may be less reliable because spin diffusion is expected to be greater for H2′ than for H1′ protons. Thus stacking interactions favor the G7 syn conformation over G4 syn, but the maximum difference in free energy is RT ln 4 or ~0.9 kcal/mol at 37 °C, assuming the G7 syn conformation is occupied 80% of the time.

Importance of Non-nearest Neighbors. The oligomer 5′GCGUGCAGGC3′ was synthesized to form a second duplex with a GG pair in the $\frac{5'A\mathbf{G}G3'}{3'U\mathbf{G}C5'}$ context. The thermodynamics of duplex formation show that the free energy per GG pair in (5′GCGUGCAGGC3′)$_2$ is +0.6 kcal/mol, similar to the +0.3 kcal/mol for (5′GCAGGCGUGC3′)$_2$ (Table 3). A 400 ms NOESY spectrum of the duplex (5′GCGUGCAGGC3′)$_2$ showed features similar to the spectrum of (5′GCAGGCGUGC3′)$_2$ (Supporting Information). For examples, the G3H1′−H8 and G8H1′−H8 cross-peaks are enlarged; the G8H1′ resonance is significantly broadened relative to other H1′ resonances, and cross-peaks are observed for U4H1′−G3H8 and G9H1′−G8H8, consistent with conformations that include syn glycosidic torsions for G3 and G8. There are additional minor cross-peaks that are not observed with (5′GCAGGCGUGC3′)$_2$, suggesting that there is a minor conformer that is in slow exchange with major conformations. Nevertheless, these data support the hypothesis that the characteristics of single GG conformational exchange are driven primarily by the context of adjacent base pairs.

Importance of Functional Groups of Watson−Crick Pairs Adjacent to GG. The identity of the adjacent base pairs may play an important role in determining the rate of swapping between the paired guanosines, and presumably the equilibrium between the two conformers. By symmetry, energies within the pair are the same for both conformations, so stacking interactions will drive any conformational preference. To test the importance of individual functional groups, oligomers with modified adjacent bases were synthesized: 5′GC^{2A}PGGCGUGC3′, 5′GCAGiGiCGUGC3′, and 5′GCAGICGUGC3′, along with the corresponding oligomers that form duplexes without mismatches: 5′GC^{2A}PGCUGC3′, 5′GCAiGiCUGC3′, and 5′GCAICUGC3′. The thermodynamics of these duplexes are shown in Table 1. The nearest-neighbor free energies have not been measured for these nucleotide analogues so we do not calculate $\Delta G^\circ_{37,\mathrm{loop}}$. The differences in free energy between duplex formation with and without the two GG pairs are +5.2, +3.4, and +3.2 kcal/mol for (5′GC^{2A}PGGCGUGC3′)$_2$, (5′GCAGiGiCGUGC3′)$_2$, and (5′GCAGICGUGC3′)$_2$, respectively, compared with +4.7 kcal/mol for (5′GCAGGCGUGC3′)$_2$.

Qualitatively, NMR spectra for the duplexes with analogues were similar to those for (5′GCAGGCGUGC3′)$_2$, although small changes in chemical shifts were observed (Supporting Information). As with (5′GCAGGCGUGC3′)$_2$, the duplexes with ^{2A}P and with iG and iC have broad G4H1′ and G7H1′ resonances, enlarged G7H1′-G7H8 NOESY cross-peaks, and the unusual R5H1′−G4H8 and U8H1′−G7H8 cross-peaks. For (5′GC^{2A}PGGCGUGC3′)$_2$, however, the G4H1′-G4H8 cross-peak is enlarged relative to the corresponding peak in (5′GCAGGCGUGC3′)$_2$ and for (5′GCAGiGiCGUGC3′)$_2$, the G4H1′-G4H8 cross-peak is attenuated. These may be due to different magnitude of exchange broadening of G4H1′ in these duplexes. Thus there are only small differences in occupation of the two conformational states and kinetics of swapping between (5′GCAGGCGUGC3′)$_2$, (5′GC^{2A}PGGCGUGC3′)$_2$, and (5′GCAGiGiCGUGC3′)$_2$. Effects due to substitution of the central GC pair with an IC pair were difficult to identify because of the significantly lower melting temperature of the duplex with an IC pair. On the basis of these data, the locations of individual functional groups on the adjacent base pairs are relatively unimportant for the equilibrium and kinetics of the swapping between the G4 syn and G7 syn conformations.

Other Orientations of Adjacent Base Pairs. Other duplexes with two single GG pairs generally had rates of conformational exchange that were unfavorable for obtaining structural information by NMR. Tables 1 and 3 contain thermodynamic data on formation of GG pairs for these contexts. One context studied is $\frac{5'G\mathbf{G}A3'}{3'C\mathbf{G}U5'}$ in (5′GAGGAUGCUC3′)$_2$. The free energy of this GG pair (Table 3) with one GC and one AU adjacent base pair is −0.95 kcal/mol, about 1 kcal/mol more favorable than for $\frac{5'A\mathbf{G}G3'}{3'U\mathbf{G}C5'}$ in (5′GCAGGCGUGC3′)$_2$. Replacement of guanosines by inosine destabilizes the duplex by about 1 kcal/mol per substitution (Table 3).

The imino proton spectrum for (5′GAGGAUGCUC3′)$_2$ shows resonances between 10 and 11 ppm that are assigned to the mismatched Gs (Supporting Information). The deriva-

tives (5′GAGIAUGCUC3′)$_2$ and (5′GAGGAUICUC3′)$_2$ each lack one or the other of these resonances, and (5′GAGIAUICUC3′)$_2$ lacks both. This may be due, in part, to the lower imino pK_a of inosine, 8.8, versus guanosine, 9.2, to faster conformational exchange with mismatches of inosine (seen with dIdI in ref 38), to structural differences, or to a combination of these effects. Resonances above 12 ppm were similar for all four duplexes.

In spectra of nonexchangeable protons for (5′GAGGAUGCUC3′)$_2$, the H5/H6 NOESY cross-peaks for U6 and C8 are considerably weaker than for U9 and C10, although H5 and H6 protons for all pyrimidines are ~2.5 Å apart (Supporting Information). Resonances from the H1′ and H8 protons from G4 and G7 are not observed. As with (5′GCGGCGC3′)$_2$ (*18*), the GG pairs in this duplex appear to be exchanging conformation at an intermediate rate, eliminating peaks in the region of the GG. Similarly, (5′GAGIAUGCUC3′)$_2$ and (5′GAGGAUICUC3′)$_2$ have attenuated cross-peaks for resonances near the mismatch site (data not shown).

The oligomer 5′CGGAGCUGCG3′, which also makes a duplex containing the $\overset{5'GGA3'}{3'CGU5'}$ context, was studied. The free energy increment attributable to each GG mispair is −0.45 kcal/mol at 37 °C, similar to the −0.95 kcal/mol for (5′GAGGAUGCUC3′)$_2$. The 400 ms mixing time NOESY spectrum shows approximately equal-sized pyrimidine H5/H6 cross-peaks for (5′CGGAGCUGCG3′)$_2$, so the exchange rate appears faster when the duplex center is stabilized by GC in addition to AU pairs and the GG mismatches are only two base pairs from a helix end. Several base protons of (5′CGGAGCUGCG3′)$_2$ resonate near 6 ppm so overlap with other cross-peaks prevents identification of A4H1′−G3H8 cross-peaks, if any, which are a signature of a syn glycosidic conformation. Nevertheless, there is a large H1′−H8 cross-peak, likely from G3 or G8, so the GG structure appears to be a syn-anti N1-carbonyl, N7-amino pairing as with (5′GCAGGCGUGC3′)$_2$.

The duplex (5′GCAGCGGUGC3′)$_2$ has the central GC pair reversed from (5′GCAGGCGUGC3′)$_2$. The base−H1′ region of the 400 ms mixing time spectrum for (5′GCAGCGGUGC3′)$_2$ at 37 °C is similar to the spectrum of Figure 7 for (5′GCAGGCGUGC3′)$_2$ (Supporting Information). The G7H1′−G7H8 cross-peak is large and the G7H1′ resonance is very broad, suggesting the GG pairing is similar regardless of the orientation of the central GC. There is, however, significant attenuation of C5 and U8 H5/H6 cross-peaks in (5′GCAGCGGUGC3′)$_2$ relative to those for C2 and C10. Additionally there are several distinct but smaller NOE cross-peaks that may be attributed to a minor conformation. The chemical shifts for nucleotides G1, C2, and C10 appear to be essentially the same for both the major and minor conformations, suggesting that the difference in geometry is at the central part of the duplex. Some minor peaks correspond to C5 and U8 H5/H6 cross-peaks, as evidenced by coupling observed with a DQF-COSY spectrum (not shown). In the NOESY spectrum, the H5/H6 cross-peak volumes are in the ratio 10:9.1:7.6:7.4 for C10:C2:U8:C5 and 1.5 and 1.3 for two minor H5/H6 cross-peaks, so the minor conformation appears to comprise ~10% of the duplexes at this temperature. Thus reversing the central GC pair in 5′GCAGGCGUGC3′ to 5′GCAGCGGUGC3′ produces slower conformational exchange and a detectable amount of a minor conformation.

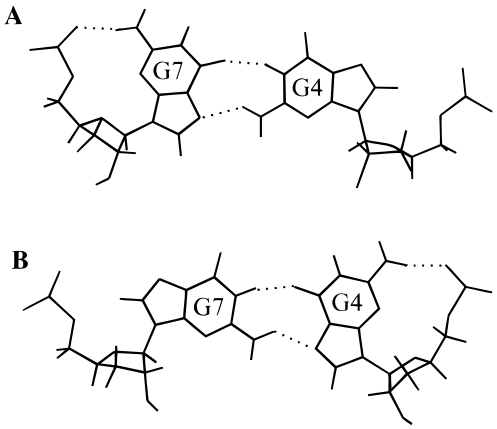

FIGURE 10: G4−G7 pair from the minimized, averaged structures of (5′GCAGGCGUGC3′)$_2$. Hydrogen bonds are shown as dotted lines. (A) GG mispair in the G7 syn structure; (B) GG mispair with G4 syn.

DISCUSSION

Structure of GG in (5′GCAGGCGUGC3′)$_2$. Figure 10 shows the final G4−G7 pairs from the two structures of (5′GCAGGCGUGC3′)$_2$. Three hydrogen bonds stabilize each pair. Two link the imino and amino donors of the anti-oriented G to the carbonyl and N7 of the syn G. Secondary electrostatic interactions between the imino group and N7, and between the amino and O6 groups may provide further stabilization (*41*). The third hydrogen bond helps fix the position of the syn G by linking the amino group with the pro-R_p, nonbridging oxygen from the 5′ phosphate of the syn G. The same amino−phosphate hydrogen bond has been observed for the *syn*-oriented G in the crystal structure of a G(syn)−A$^+$ pair (*42*). A 2-amino−5′-phosphate interaction is also imputed in producing the syn glycosidic geometries for guanosine mononucleotides, which are observed both in solution and in crystals (*43*).

The N1-carbonyl, N7-amino pair is compatible with a Watson−Crick helix (*14*), as illustrated in Figure 1C. The C1′−C1′ distances for the G4−G7 pairs are both 11.5 Å, slightly larger than the 10.7 Å for G1−C10 and C2−G9 in the duplex and the 10.6−10.7 Å in the crystal structure of a Watson−Crick helix at 1.2 Å resolution (*44*). The A3−U8 and G5−C6 pairs adjacent to G4−G7 have a slightly enlarged C1′−C1′ distance of 10.9−11.0 Å. The angles made by the glycosidic bonds and the line connecting the C1′ atoms are ~28° for the syn guanosine and ~75° for the anti guanosine. Although these differ significantly from the ~57° and ~51° for C2 and G9, respectively, the sum of the two angles, which gives an indication of helical twist, are close for the G4−G7 pair and the Watson−Crick C2−G9 pair. Thus the GG pair is slightly larger, but it does not significantly alter the backbone of the A-form helix. As discussed below, the structures of the GG pairs in (5′GCAGGCGUGC3′)$_2$ provide rationales for the observations that stabilities of GG pairs are more favorable (*16*−*18*) and less dependent on distance from a helix end (*18*) than are stabilities of other mismatches.

Conformational Exchange. Exchange between two conformations can be described by thermodynamics, which

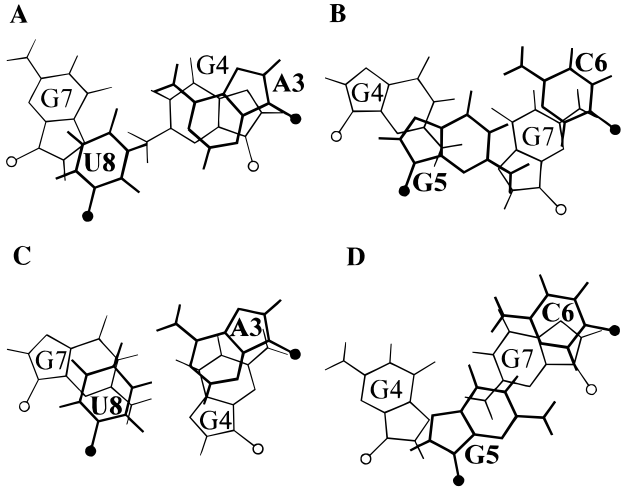

FIGURE 11: Overlaps between the GG pair and the adjacent Watson−Crick pairs. (A) G4−G7 syn and A3−U8. (B) G4−G7 syn and G5−C6; (C) G4 syn−G7 and A3−U8; (D) G4 syn−G7 and G5−C6.

determines the occupation of the two conformations, and by kinetics, which determines the rate of exchange. For (5′GCAGGCGUGC3′)$_2$ the thermodynamic preference for G7 to be in the syn conformation is likely to stem from stacking interactions with adjacent pairs because, within the GG pair, the two structures are equivalent.

Figure 11 shows the overlaps of the GG pairs with adjacent Watson−Crick pairs. The top and bottom panels show overlaps for the G7 syn and G4 syn structures, respectively. For the G7 syn structure, with G4 in the anti position, there is appreciable overlap between the G4 and A3 bases (panel A); there is less overlap between purines for the G4 syn structure (panel C). An unfavorable stacking interaction for G4 syn can be seen in Figure 11D: the negatively charged regions of G4 and G5, composed of the N7 and carbonyl groups, overlap directly. This unfavorable interaction is relieved when G4 is in the anti conformation (Figure 11B). Similar guanine overlaps appear to govern stability and structure of GA and GU pairs (*8*, *45*, *46*).

A lower limit can be placed on the rate of exchange, k, between the G4 syn and G7 syn conformations. The characteristics of NMR resonances of an exchanging system depend on the ratio of exchange rate to the difference in resonance frequencies of a given nucleus for the two environments (*47*). The observation of a single set of peaks indicates fast exchange, so $k \gg (\nu_A - \nu_B)$ where $(\nu_A - \nu_B)$ is the difference in resonance frequencies of a given proton for the two conformations. A conservative estimate for the maximum chemical shift difference in (5′GCAGGCGUGC3′)$_2$ is 0.4 ppm or 200 Hz on a 500 MHz instrument, so the characteristic rate of swapping between G4 syn and G7 syn is on the order of 10^3 s^{-1} or faster at 37 °C. Given the equilibrium constant of $\exp[-\Delta G°_{37}/RT] = \exp\{9.15 \times 10^3/[(1.987)(310)]\} = 2.8 \times 10^6$ for duplex formation in 1 M NaCl at 37 °C (Table 1), and an expected association rate constant of $\sim 10^6$ M^{-1} s^{-1}, the rate for strand dissociation is likely on the order of 1 s^{-1}. Thus, swapping of G4 syn and G7 syn probably does not require strand dissociation.

Thermodynamics of Single GG Pairs. The free energies attributable to each GG pair in (5′GCAGGCGUGC3′)$_2$ and (5′GCGUGCAGGC)$_2$ are +0.3 and +0.6 kcal/mol, respectively. On the basis of a current model that depends only on the identity of the adjacent Watson−Crick pairs (*18*), the $\Delta G°_{37,\text{loop}}$ of $^{5'\mathbf{A}\mathbf{G}3'}_{3'\mathbf{U}\mathbf{G}5'}$ is expected to be −1.4 kcal/mol. Thus, the GG pairs in these duplexes are 1.7 and 2.0 kcal/mol less stable than expected. Similarly, (5′GCAGCGGUGC3′)$_2$ provides less free energy than expected, −0.2 kcal/mol. In contrast, the free energy increments for each GG pair in (5′GAGGAUGCUC3′)$_2$ and (5′GACGAUGGUC3′)$_2$ are −0.95 and −1.4 kcal/mol, respectively (Table 3), close to the expected value of −1.4 kcal/mol. It is unclear why single GG pairs are less stable than expected in some contexts. Perhaps the stacking interaction $^{5'\mathbf{A}\mathbf{G}3'}_{3'\mathbf{U}\mathbf{G}5'}$ is particularly unfavorable. If so, this does not stem from the location of the amino group on A as $^{5'^{2\mathrm{A}}\mathbf{P}\mathbf{G}3'}_{3'\ \ \mathbf{U}\mathbf{G}5'}$ has a similar unfavorable free energy. Since G has a large dipole moment, stacking interactions with GG pairs may be especially sensitive to adjacent pairs.

We note that sequences with less favorable free energy increments for GG are generally more suitable for NMR structural determination. For example, $^{5'\mathbf{A}\mathbf{G}3'}_{3'\mathbf{U}\mathbf{G}5'}$ has an average free energy increment of +0.4 kcal/mol and NMR resonances for the mismatched region are observed, whereas $^{5'\mathbf{G}\mathbf{G}3'}_{3'\mathbf{C}\mathbf{G}5'}$ has an increment of −1.9 kcal/mol and resonances near the mismatch site are not observed (*18*). Perhaps a higher ground-state energy for contexts such as $^{5'\mathbf{A}\mathbf{G}3'}_{3'\mathbf{U}\mathbf{G}5'}$ allow the transition state for exchange to be reached more readily, thereby making exchange fast enough that resonances are not overly broadened. Additionally, the transition-state energy may be lower for $^{5'\mathbf{A}\mathbf{G}3'}_{3'\mathbf{U}\mathbf{G}5'}$ than for $^{5'\mathbf{G}\mathbf{G}3'}_{3'\mathbf{C}\mathbf{G}5'}$ because of the smaller penalty for disrupting an AU than a GC pair and potential favorable interactions of the mismatched Gs with A or U in the transition state.

The N1-carbonyl, N7-amino GG structure of Figure 10 rationalizes thermodynamic effects observed upon substitutions of inosine for guanosine in (5′GCAGGCGUGC3′)$_2$. The amino group of each guanosine is involved in hydrogen bonds, so replacement of either with inosine is expected to destabilize the duplex. Furthermore, if there is a thermodynamic preference for the G7 syn structure, the effect of replacing the G4 with inosine is expected to differ from the effect of replacement of G7. Replacement of G7 with I, and thus removal of the hydrogen bond to the phosphate in the preferred conformation, destabilizes each mismatch in the duplex by nearly 1 kcal/mol (Table 3; Figure 5) but appears to have a small effect on structure, since chemical shifts are similar for the G4−I7 and the G4−G7 duplexes (NOESY spectra for the duplexes with GI and IG mismatches are provided in Supporting Information). In contrast, replacement of G4 with inosine appears to change the structure, as the melting profile (Figure 5) and chemical shifts (NOESY spectrum in Supporting Information) are much different for the IG and GG duplexes. This suggests the two hydrogen bonds between the Gs are required to maintain the structure, but the hydrogen bond to the phosphate is not.

The N1-Carbonyl, Amino-N7 Syn-Anti Structure Is Probably General for Single GG. Qualitatively, the imino proton resonances of the noncanonically paired Gs in (5′GCAGGCGUGC3′)$_2$ (Figure 6) are consistent with the GG structure of Figure 1C. Similarly, GG pairs in other contexts show one sharp and one broader resonance between 10 and 12

ppm (Figure 4A; *18*). This suggests that only one imino proton is hydrogen-bonded and thus is consistent with either the syn−anti Figure 1C or the anti−anti Figure 1D pairing in these contexts. The syn−anti structure of Figure 1C is also supported for the $^{5'G\mathbf{G}C3'}_{3'C\mathbf{G}G5'}$ context by the effect of helix position on stability. Unlike AA and UU mismatches, the stability of a single GG mismatch is independent of position in a helix (*18*). This is expected for pairs, such as the syn−anti N1-carbonyl, N7-amino GG structure, which are nearly isosteric with Watson−Crick pairs. Such pairs require minimal helical distortion even when placed at the helix center.

The GG pair conformation in Figure 1C is also consistent with the thermodynamic effects of substituting I and 7dG in a GG pair in the context $^{5'G\mathbf{G}C3'}_{3'C\mathbf{G}G5'}$ (Table 2). The local symmetry of $^{5'G\mathbf{G}C3'}_{3'C\mathbf{G}G5'}$ allows the two Gs to swap anti and syn without preference for one conformation. Replacement of either G with I destabilizes the mismatch by 0.6 kcal/mol. This effect could largely be due to breaking of local sequence symmetry. If I is preferred in the syn conformation, for instance, available conformations are reduced by half, and free energy becomes less favorable by *RT* ln 2, or 0.4 kcal/mol at 37 °C. Furthermore, one hydrogen bond of a GG pair would be sacrificed with GI, either a hydrogen bond with the phosphate if I is syn or the amino−N7 hydrogen bond if I is in the anti conformation (presumably the weaker bond will be disrupted). Given these considerations alone, it is perhaps surprising that the destabilization for GI relative to GG is only 0.6 kcal/mol. Other factors can mitigate the destabilization, however: (a) The I imino proton is more acidic than that of G (pK_a 8.8 vs 9.2) so a hydrogen bond involving this proton will be stronger for GI than for GG. (b) When a hydrogen-bonding group is eliminated, changes in geometry and solvation can lead to stabilizing interactions, as seen with RNA tetraloops (*48, 49*). Such a structural difference is suggested by the large downfield shift of the I imino proton in $^{5'GUG\mathbf{I}CAG3'}_{3'CAC\mathbf{G}GUC5'}$ relative to GG shifts in $^{5'GUG\mathbf{G}CAG3'}_{3'CAC\mathbf{G}GUC5'}$ (Figure 4A,B). On the basis of these considerations, replacing an N1-carbonyl, N7-amino GG pair of Figure 1C with an II mismatch is expected to eliminate two hydrogen bonds. Such a loss is consistent with the observed loss of 1.5 kcal/mol in free energy for the GG to II substitution.

For mismatches with 7dG, destabilizations are more dramatic. Only one N7 is involved in a hydrogen bond in the Figure 1C GG pair, so a G−7dG pair will allow the three hydrogen bonds to remain but will require the 7dG to be in anti conformation and the G to be syn. This reduces the number of available conformations by half, making the expected free energy 0.4 kcal/mol less favorable at 37 °C. The reduction in available conformations explains only some of the ∼1 kcal/mol destabilization observed for a G−7dG or 7dG−G pair. The pK_a of the imino proton for 7dG is ∼10.3 (*35*), however, whereas it is 9.2 for G. Thus the imino proton in 7dG will produce weaker hydrogen bonds. This can account for the additional 0.6 kcal/mol destabilization seen with a G to 7dG substitution.

Since 7dG is likely to occupy the anti position in a pair with guanosine or inosine, the difference in stabilities of G−7dG and I−7dG provide an estimate of the amino−phosphate hydrogen-bond stability, ∼0.8 kcal/mol for the GG two or three base pairs from a helix end (Table 2). This is close to the ∼1.1 kcal/mol destabilization per mismatch for 5′GCA**G**GC**I**UGC3′ relative to 5′GCA**G**GC**G**UGC3′.

The above comparisons indicate that a syn−anti GG pair, where the two Gs can swap positions in the pair, is a reasonable model to explain the thermodynamic and NMR data for several sequences. Nevertheless, minor conformers with other GG structures are possible.

Thermodynamics for Mismatches Near Helix Termini. Kierzek et al. (*18*) showed that, in contrast to AA and UU mismatches, stability of a single GG is unaffected by the number of base pairs separating it from a helix end. The data for mismatches including I and 7dG in Table 2, however, illustrate that less-stable mispairs with these analogues are affected appreciably by position in the duplex. Whereas I−I and 7dG−7dG mismatches fall ∼0.6 kcal/mol short of the stability of GG even 1 bp from an end, they are stabilized by 1.1 and over 3 kcal/mol, respectively, when moved from 3 bp to 1 bp from an end. A similar stabilization of 1.1 kcal/mol has been observed for AA mismatches (*18*). Possibly the additional flexibility near the end of the helix allows I−I, 7dG−7dG, and A−A to achieve a more stable conformation with little disruption of the helical structure of the rest of the duplex.

Known RNA Structures with Various GG Pairs. Structures with guanosine-guanosine mispairs have been observed in contexts other than single mismatches. Crystal structures of free Rev-responsive element (RRE) RNA show the Figure 1C structure, with the syn G next to a bulged U (*50, 51*). When Rev is bound, models of the RRE based on NMR show that a GG pair in a 3 × 2 nucleotide internal loop forms two N1-carbonyl hydrogen bonds, as shown in Figure 1A (*1, 2*). Because AA, AC, and GU pairs are partially compatible with Rev binding, Leontis and Westhof (*14*) propose that the actual GG structure with Rev bound may be an anti−anti pair similar to Figure 1D but with a bifurcated hydrogen bond from the carbonyl of one G to the imino and amino groups of the other. This bifurcated GG pair has been observed for a GG flanked by reverse Hoogsteen AU and an imino-hydrogen-bonded GA in the crystal structure of a 5S rRNA domain (*15*). Thus the geometry adopted by a GG pair can depend on adjacent pairs, unpaired nucleotides, and on binding by ligands.

In other contexts, GG pairs have been observed with anti−anti and syn−anti geometries. In the HDV antigenomic ribozyme, an N1-carbonyl, symmetric pair is postulated as critical for function (*12*). In an ATP-binding aptamer, found by in vitro selection, two GG pairs form (*9, 10*); one is an anti−anti N7 carbonyl, N1 amino pair (Figure 1D) and the second is an N1-carbonyl, N7-amino syn−anti pair (Figure 1C). In the secondary structure, the syn G of the second pair is sandwiched between two helixes, and in three dimensions it is stacked 3′ to the A of an AU pair. The syn G amino group in the ATP aptamer approaches its 5′-phosphate oxygen close enough to form a hydrogen bond (*9, 10*) and the structure is similar to that observed here in a continuous helix. Similarly, the related RNA aptamers for arginine and citrulline each contain an N1-carbonyl, N7-amino syn−anti pair (Figure 1C) when their corresponding ligands are bound (*11*).

Shah and Brünger (*52*) crystallized an RNA duplex containing a single GG in the context $^{5'U\mathbf{G}G3'}_{3'G\mathbf{G}U5'}$, but statistical disorder in the crystal prevented observation of a clear GG pairing pattern. Because the GG pair is at the center of a self-complementary duplex, it is likely that either G can adopt a syn conformation with equal probability. Although active flipping is unlikely in a crystal, random orientation of the two Gs may have added to the statistical disorder observed in the crystal. The crystal structure of the signal recognition particle (SRP) core contains an anti−anti GG linked by a single amino−carbonyl hydrogen bond (*53*). The GG is flanked by an imino-hydrogen-bonded GA pair and by an AC pair, and one of the Gs makes contact with the associated polypeptide. As a whole, these observations suggest that the Figure 1C pair is preferred as a single GG pair or in a constrained context and that other GG pairings occur in other contexts.

Single dGdG Mispairs in DNA. In DNA, single dGdG pairs in a continuous helix have been the object of several structural studies. As with RNA, single dGdG pairs are more stable than other mismatches (*54*, *19*) and dynamic in structure (*39*). Identification of a particular GG structure was impeded by the conformational exchange. Cognet et al. (*55*) used NMR data to model dGdG in the context $^{5'A\mathbf{G}G3'}_{3'TGC5'}$ and concluded that the mismatch forms an N1-carbonyl, symmetric syn−anti pair (Figure 1A), although there was no strong evidence to rule out the Figure 1C pairing or an intermediate bifurcated pair. As with r(5′GCAGGCGUGC3′)$_2$, this context has a rate of conformational exchange that is favorable for NMR and the dG surrounded by pyrimidines prefers the syn conformation.

Other contexts of dGdG exhibit extreme broadening of resonances near the mismatch site, making interpretation difficult. Borden et al. (*56*) studied dGdG in the context $^{5'C\mathbf{G}A3'}_{3'G\mathbf{G}T5'}$ and developed a model with both dGs in the anti conformation with weak hydrogen bonding, but there was considerable conformational heterogeneity near the mismatch and models with a syn G were only slightly disfavored in molecular modeling. Faibis et al. (*57*) also studied dGdG in the $^{5'C\mathbf{G}A3'}_{3'G\mathbf{G}T5'}$ context and developed a model with an anti−anti dG pair with a single amino−carbonyl hydrogen bond. Both Borden et al. (*56*) and Faibis et al. (*57*) chose an anti−anti model because the mismatched dGs had normal-sized H1′−H8 NOEs, which were expected to be enlarged for a syn conformation. Exchange of individual dGs between the syn and anti conformations and the resulting line broadening, however, may produce H1′−H8 NOE cross-peaks that do not appear enlarged. Lane and Peck (*39*) also studied dGdG in the $^{5'C\mathbf{G}A3'}_{3'G\mathbf{G}T5'}$ context by NMR, but despite the size of H1′−H8 cross-peaks, they concluded that the dGdG was syn−anti because of a larger ratio of H1′−H8 to H1′−H2″ NOE volumes than for anti nucleotides. A crystal structure by Skelly et al. (*58*) with dGdG in the context $^{5'C\mathbf{G}A3'}_{3'G\mathbf{G}T5'}$ identified a syn−anti dGdG pairing scheme similar to Figure 1C. Critical examination of these papers suggests that, in solution, the Figure 1C syn−anti pairing is likely for DNA with the $^{5'C\mathbf{G}A3'}_{3'G\mathbf{G}T5'}$ context, although it is possible that the mismatch structure is highly dependent on conditions of temperature, salt, and nonadjacent nucleotides.

In DNA, dGdG mismatches have also been studied in other contexts. Lane and Peck (*39*) conclude that the pair is in a syn−anti conformation in $^{5'C\mathbf{G}G3'}_{3'G\mathbf{G}C5'}$ and $^{5'C\mathbf{G}A3'}_{3'G\mathbf{G}T5'}$ with the dGs exchanging position in the pair, but conformational exchange made it difficult to identify the exact nature of the dGdG pair. On the basis of biochemical and enzymatic mapping, Mitas et al. (*59*) conclude that dGdG in $^{5'C\mathbf{G}G3'}_{3'G\mathbf{G}C5'}$ is in the Figure 1C syn−anti dGdG conformation and that the two dGs interchange positions. Thus the syn−anti N1-carbonyl, N7-amino dGdG pair occurs in single mismatches of DNA, in several contexts.

Occurrence of GG in Known Secondary Structures. A search of a database of large subunit rRNA secondary structures (*60*) reveals that, of 196 GG pairs flanked by Watson−Crick pairs, the motif $^{5'A\mathbf{G}G3'}_{3'U\mathbf{G}C5'}$ studied here occurs 40 times at position G1360−G1371 (*Escherichia coli* numbering) in bacterial and chloroplast large-subunit rRNAs. For these sequences, an AG mispair is usually adjacent to the AU pair, so it is possible that the AU is not Watson−Crick. Nevertheless, the conservation suggests that this site is important for function in these organisms.

A single N1-carbonyl, N7-amino GG mismatch (Figure 1C) may be a good site for specific binding or tertiary contacts. The pair positions two adjacent hydrogen-bond donors and two adjacent acceptors in the major groove. Thus, it has the ability to form four hydrogen bonds at this site. For example, it is possible for another GG pair to make the hydrogen bonds, forming a quartet structure. Conformational degeneracy of a single GG may help confer binding specificity as weak binding will not overcome the entropic penalty of fixing the mismatch. The large dipole moments, adjacent hydrogen-bonding groups, and conformational degeneracy may make GG pairs good targets for pharmacological agents.

ACKNOWLEDGMENT

We thank T. R. Krugh, M. A. Fountain, T. Xia, and X. Chen for helpful discussions.

SUPPORTING INFORMATION AVAILABLE

Four tables of NMR assignments, distance restraints, torsion restraints, and refinement details and 20 figures showing the DQF-COSY and NOESY spectra for (5′GCAGGCGUGC3′)$_2$; 1D NOE spectra of $^{5'GUG\mathbf{I}CAG3'}_{3'CAC\mathbf{G}GUC5'}$ and $^{5'G\mathbf{I}C\underline{U}GAG3'}_{3'C\mathbf{I}GACUC5'}$; the base−base region of the NOESY spectrum of (5′GCAGGCGUGC3′)$_2$, base−H1′ regions of NOESY spectra for (5′GCGUGCAGGC3′)$_2$, (5′GC^{2A}PGGCGUGC3′)$_2$, (5′GCAGiGiCGUGC3′)$_2$, (5′GAGGAUGCUC3′)$_2$, (5′CGGAGCUGCG3′)$_2$, (5′GCAGCGGUGC3′)$_2$, (5′GCAIGCGUGC3′)$_2$, and (5′GCAGGCIUGC3′)$_2$; 1D imino proton spectra of (5′GAGGAUGCUC3′)$_2$, (5′GAGIAUGCUC3′)$_2$, (5′GAGGAUICUC3′)$_2$, and (5′GAGIAUICUC3′)$_2$; and van't Hoff plots for melting experiments. This material is available free of charge via the Internet at http://pubs.acs.org.

REFERENCES

1. Peterson, R. D., and Feigon, J. (1996) *J. Mol. Biol. 264*, 863−877.
2. Battiste, J. L., Mao, H., Rao, N. S., Tan, R., Muhandiram, D. R., Kay, L. E., Frankel, A. D., and Williamson, J. R. (1996) *Science 273*, 1547−1551.
3. Mathews, D. H., Sabina, J., Zuker, M., and Turner, D. H. (1999) *J. Mol. Biol. 288*, 911−940.

4. Wu, M., McDowell, J. A., and Turner, D. H. (1995) *Biochemistry 34*, 3204−3211.
5. Xia, T., McDowell, J. A., and Turner, D. H. (1997) *Biochemistry 36*, 12486−12497.
6. Walter, A. E., Wu, M., and Turner, D. H. (1994) *Biochemistry 33*, 11349−11354.
7. SantaLucia, J., Jr., and Turner, D. H. (1993) *Biochemistry 32*, 12612−12623.
8. Wu, M., and Turner, D. H. (1996) *Biochemistry 35*, 9677−9689.
9. Dieckmann, T., Suzuki, E., Nakamura, G. K., and Feigon, J. (1996) *RNA 2*, 628−640.
10. Jiang, F., Kumar, R. A., Jones, R. A., and Patel, D. J. (1996) *Nature 382*, 183−186.
11. Yang, Y., Kochoyan, M., Burgstaller, P., Westhof, E., and Famulok, M. (1996) *Science 272*, 1343−1347.
12. Been, M. D., and Perrotta, A. T. (1995) *RNA 1*, 1061−1070.
13. Burkard, M. E., Turner, D. H., and Tinoco, I., Jr. (1999) in *The RNA World* (Gesteland, R. F., Cech, T. R., and Atkins, J. F., Eds.) pp 675−680, Cold Spring Harbor Laboratory Press, Cold Spring Harbor, NY.
14. Leontis, N. B., and Westhof, E. (1998) *Q. Rev. Biophys. 31*, 399−455.
15. Correll, C. C., Freeborn, B., Moore, P. B., and Steitz, T. A. (1997) *Cell 91*, 705−712.
16. Zhu, J., and Wartell, R. M. (1997) *Biochemistry 36*, 15326−15335.
17. Bevilacqua, J. M., and Bevilacqua, P. C. (1998) *Biochemistry 37*, 15877−15884.
18. Kierzek, R., Burkard, M. E., and Turner, D. H. (1999) *Biochemistry 38*, 14214−14223.
19. Peyret, N., Seneviratne, P. A., Allawi, H. T., and SantaLucia, J., Jr. (1999) *Biochemistry 38*, 3468−3477.
20. Kierzek, R., Caruthers, M. H., Longfellow, C. E., Swinton, D., Turner, D. H., and Freier, S. M. (1986) *Biochemistry 25*, 7840−7846.
21. Usman, N., Ogilvie, K. K., Jiang, M.-Y., and Cedergren, R. J. (1987) *J. Am. Chem. Soc. 109*, 7845−7854.
22. Wincott, F., DiRenzo, A., Shaffer, C., Grimm, S., Tracz, D., Workman, C., Sweedler, D., Gonzalez, C., Scaringe, S., and Usman, N. (1995) *Nucleic Acids Res. 23*, 2677−2684.
23. Stawinski, J., Stromberg, R., Thelin, M., and Westman, E. (1988) *Nucleic Acids Res. 16*, 9285−9298.
24. Richards, E. G. (1975) in *Handbook of Biochemistry and Molecular Biology: Nucleic Acids—Volume I.* (Fasman, G. D., Ed.) 3rd ed., p 597, CRC Press, Cleveland, OH.
25. Borer, P. N. (1975) in *Handbook of Biochemistry and Molecular Biology: Nucleic Acids—Volume I.* (Fasman, G. D., Ed.) 3rd ed., p 589, CRC Press, Cleveland, OH.
26. Peritz, A. E., Kierzek, R., Sugimoto, N., and Turner, D. H. (1991) *Biochemistry 30*, 6428−6436.
27. McDowell, J. A., and Turner, D. H. (1996) *Biochemistry 35*, 14077−14089.
28. Borer, P. N., Dengler, B., Tinoco, I., Jr., and Uhlenbeck, O. C. (1974) *J. Mol. Biol. 86*, 843−853.
29. Hore, P. J. (1983) *J. Magn. Reson. 55*, 283−300.
30. Sklenar, V., Miyashiro, H., Zon, G., Miles, H. T., and Bax, A. (1986) *FEBS Lett. 208*, 94−98.
31. Cornell, W. D., Cieplak, P., Bayly, C. I., Gould, I. R., Merz, K. M., Jr., Ferguson, D. M., Spellmeyer, D. C., Fox, T., Caldwell, J. W., and Kollman, P. A. (1995) *J. Am. Chem. Soc. 117*, 5179−5197.
32. Schmidt, M. W., Baldridge, K. K., Boatz, J. A., Elbert, S. T., Gordon, M. S., Jensen, J. H., Koseki, S., Matsunaga, N., Nguyen, K. A., Su, S., Windus, T. L., Dupuis, M., and Montgomery, J. A., Jr. (1993) *J. Comput. Chem. 14*, 1347−1363.
33. Fogarasi, G., Zhou, X., Taylor, P. W., and Pulay, P. (1992) *J. Am. Chem. Soc. 114*, 8191−8201.
34. Xia, T., SantaLucia, J., Jr., Burkard, M. E., Kierzek, R., Schroeder, S. J., Jiao, X., Cox, C., and Turner, D. H. (1998) *Biochemistry 37*, 14719−14735.
35. Ramzaeva, N., and Seela, F. (1996) *Helv. Chim. Acta 79*, 1549−1558.
36. Burkard, M. E., Kierzek, R., and Turner, D. H. (1999) *J. Mol. Biol. 290*, 967−982.
37. Hirschfelder, J. O., Curtiss, C. F., and Bird, R. B. (1954) *Molecular Theory of Gases and Liquids*, pp 960−964, John Wiley & Sons, New York.
38. Faibis, V., Cognet, J. A. H., Boulard, Y., Sowers, L. C., and Fazakerley, G. V. (1996) *Biochemistry 35*, 14452−14464.
39. Lane, A. N., and Peck, B. (1995) *Eur. J. Biochem. 230*, 1073−1087.
40. Bonvin, A. M., and Brünger, A. T. (1996) *J. Biomol. NMR 7*, 72−76.
41. Pranata, J., Wierschke, S. G., and Jorgensen, W. L. (1991) *J. Am. Chem. Soc. 113*, 2810−2819.
42. Pan, B., Mitra, S. N., and Sundaralingam M. (1999) *Biochemistry 38*, 2826−2831.
43. Saenger, W. (1984) *Principles of Nucleic Acid Structure*, pp 77−78, Springer-Verlag, New York.
44. Klosterman, P. S., Shah, S. A., and Steitz, T. A. (1999) *Biochemistry 38*, 14784−14792.
45. McDowell, J. A., He, L., Chen, X., and Turner, D. H. (1997) *Biochemistry 36*, 8030−8038.
46. Chen, X., McDowell, J. A., Kierzek, R., Krugh, T. R., and Turner, D. H. (2000) *Biochemistry 30*, 8970−8982.
47. Lian, L. Y., and Roberts, G. C. K. (1993) Effects of chemical exchange on NMR spectra, in *NMR of macromolecules: a practical approach* (Roberts, G. C. K., Ed.) Oxford University Press: New York.
48. Jucker, F. M., Heus, H. A., Yip, P. F., Moors, E. H. M., and Pardi, A. (1996) *J. Mol. Biol. 264*, 968−980.
49. SantaLucia, J., Jr., Kierzek R., and Turner, D. H. (1992) *Science 256*, 217−219.
50. Ippolito, J. A., and Steitz, T. A. (2000) *J. Mol. Biol. 295*, 711−717.
51. Hung, L.-W., Holbrook, E. L., and Holbrook, S. R. (2000) *Proc. Natl. Acad. Sci. U.S.A. 97*, 5107−5112.
52. Shah, S. A., and Brünger, A. T. (1999) *J. Mol. Biol. 285*, 1577−1588.
53. Batey, R. T., Rambo, R. P., Lucast, L., Rha, B., and Doudna, J. A. (2000) *Science 287*, 1232−1239.
54. Aboul-ela, F., Koh, D., Tinoco, I., Jr., and Martin, F. H. (1985) *Nucleic Acids Res. 13*, 4811−4824.
55. Cognet, J. A. H., Gabarro-Arpa, J., Le Bret, M., van der Marel, G. A., van Boom, J. H., and Fazakerley, G. V. (1991) *Nucleic Acids Res. 19*, 6771−6779.
56. Borden, K. L. B., Jenkins, T. C., Skelly, J. V., Brown, T., and Lane, A. N. (1992) *Biochemistry 31*, 5411−5422.
57. Faibis, V., Cognet, J. A. H., Boulard, Y., Sowers, L. C., and Fazakerley, G. V. (1996) *Biochemistry 35*, 14452−14464.
58. Skelly, J. V., Edwards, K. J., Jenkins, T. C., and Neidle, S. (1993) *Proc. Natl. Acad. Sci. U.S.A. 90*, 804−808.
59. Mitas, M., Yu, A., Dill, J., and Haworth, I. S. (1995) *Biochemistry 34*, 12803−12811.
60. Gutell, R. R., Gray, M. W., and Schnare, M. N. (1993) *Nucleic Acids Res. 21*, 3055−3074.
61. Freier, S. M., Sugiomoto, N., Sinclair, A., Alkema, D., Neilson, T., Kierzek, R., Caruthers, M. H., and Turner, D. H. (1986) *Biochemistry 25*, 3214−3219.
62. Garner, P., and Ramakanth, S. (1988) *J. Org. Chem. 53*, 1294−1298.
63. Voelter, W., Records, R., Bunnenberg, E., and Djerassi, C. (1968) *J. Am. Chem. Soc. 90*, 6163−6170.
64. Ramasamy, K., Imamura, N., Robins, R. K., and Revankar, G, R. (1988) *J. Heterocyclic Chem. 25*, 1893−1898.

BI000720I